

AN EFFICIENT ALGORITHM FOR SIMULATING ENSEMBLES OF PARAMETERIZED MHD FLOW PROBLEMS

M. MOHEBUJJAMAN^{*†}, H. WANG^{*}, L. REBHOLZ[‡], AND M. A. A. MAHBUB[§]

Abstract. In this paper, we propose, analyze, and test an efficient algorithm for computing ensemble average of incompressible magnetohydrodynamics (MHD) flows, where instances/members correspond to varying kinematic viscosity, magnetic diffusivity, body forces, and initial conditions. The algorithm is decoupled in Elsässer variables and permits a shared coefficient matrix for all members at each time-step. Thus, the algorithm is much more computationally efficient than separately computing simulations for each member using usual MHD algorithms. We prove the proposed algorithm is unconditionally stable and convergent. Several numerical tests are given to support the predicted convergence rates. Finally, we test the proposed scheme and observe how the physical behavior changes as the coupling number increases in a lid-driven cavity problem with mean Reynolds number $Re \approx 15000$, and as the deviation of uncertainties in the initial and boundary conditions increases in a channel flow past a step problem.

Key words. magnetohydrodynamics, uncertainty quantification, fast ensemble calculation, finite element method, Elsässer variables

Mathematics Subject Classifications (2000): 65M12, 65M22, 65M60, 76W05

1. Introduction. In this work, we consider the following set of J time-dependent, viscoresistive and incompressible dimensionless magnetohydrodynamics (MHD) equations [4, 6, 26, 35] for computing a MHD flow ensemble simulation of homogeneous Newtonian fluids:

$$\mathbf{u}_{j,t} + \mathbf{u}_j \cdot \nabla \mathbf{u}_j - s \mathbf{B}_j \cdot \nabla \mathbf{B}_j - \nu_j \Delta \mathbf{u}_j + \nabla p_j = \mathbf{f}_j(\mathbf{x}, t), \quad \text{in } \Omega \times (0, T], \quad (1.1)$$

$$\mathbf{B}_{j,t} + \mathbf{u}_j \cdot \nabla \mathbf{B}_j - \mathbf{B}_j \cdot \nabla \mathbf{u}_j - \nu_{m,j} \Delta \mathbf{B}_j + \nabla \lambda_j = \nabla \times \mathbf{g}_j(\mathbf{x}, t), \quad \text{in } \Omega \times (0, T], \quad (1.2)$$

$$\nabla \cdot \mathbf{u}_j = 0, \quad \text{in } \Omega \times (0, T], \quad (1.3)$$

$$\nabla \cdot \mathbf{B}_j = 0, \quad \text{in } \Omega \times (0, T], \quad (1.4)$$

$$\mathbf{u}_j(\mathbf{x}, 0) = \mathbf{u}_j^0(\mathbf{x}), \quad \text{in } \Omega, \quad (1.5)$$

$$\mathbf{B}_j(\mathbf{x}, 0) = \mathbf{B}_j^0(\mathbf{x}), \quad \text{in } \Omega, \quad (1.6)$$

where \mathbf{u}_j , \mathbf{B}_j , p_j , and λ_j denote the velocity, magnetic field, pressure, and artificial magnetic pressure solutions, respectively, for each $j = 1, 2, \dots, J$, corresponding to distinct combination of kinematic viscosity ν_j , magnetic diffusivity $\nu_{m,j}$, body force \mathbf{f}_j , $\nabla \times \mathbf{g}_j$, and initial conditions \mathbf{u}_j^0 , \mathbf{B}_j^0 . The symbol Ω denotes the simulation domain (which we assume to be convex), t the time variable, \mathbf{x} the spatial variable and T the simulation time. The coupling number s is the coefficient of the Lorentz force into the momentum equation (1.1). For simplicity of our analysis, we consider homogeneous Dirichlet boundary conditions.

Input data, e.g., initial and boundary conditions, viscosities, and body forces have a significant effect on simulations of complex dynamical systems, but the involvement of uncertainty in their measurements reduces the accuracy of final solutions. For a robust and high fidelity solution, computation of ensemble average solution is popular in many applications such as surface data assimilation [9], magnetohydrodynamics [23], porous media flow [22], weather forecasting [29, 31], spectral methods [32], sensitivity analyses [33], and hydrology [40]. Computing a quantity of interest by running a simulation subject to the ensemble average of a particular input data is not always the same as computing the ensemble average of the quantity of interest running the simulations for all different realizations of the input data first and then taking their average [11].

Computing long-time simulations of a fully coupled MHD ensemble systems is computationally arduous and expensive. Therefore, decoupled algorithms which can reuse the global system matrix at each time-step for all J realizations are computationally attractive. First-order time-stepping partitioned algorithms with small time-step restrictions are studied at low magnetic Reynolds number in a reduced MHD system in [23]. Decoupled, and unconditionally stable algorithm for the evolutionary full MHD ensemble system in Elsässer variables are investigated in [35].

^{*}Department of Mathematics and Physics, Texas A&M International University, TX 78041, USA;

[†]Correspondence: m.mohebujjaman@tamiu.edu

[‡]School of Mathematical and Statistical Sciences, Clemson University, Clemson, SC 29634, USA;

[§]Department of Mathematics, Comilla University, Cumilla 3506, Bangladesh;

Viscosity parameters are the most important and sensitive input data, as they determine the flow characteristics. For example, as the Reynolds number $Re := UL/\nu$ grows, the laminar flow moves into a convective dominated regime and eventually becomes turbulent [46]. The situation is more complex in MHD flow with high magnetic Reynolds number $Re_m := UL/\nu_m$. Here, the contribution of the nonlinearity dominates the flow's development and evolution. Thus, for an accurate simulation, it is important to accurately account for their uncertainties. The above mentioned MHD ensemble works [23, 35] were done assuming uncertainties only on the initial and boundary conditions, and forcing functions; no uncertainties are considered on the viscosity coefficients. In this paper, we propose an algorithm for the MHD flow ensemble in which not only the initial and boundary data, and forcing functions, but also the kinematic viscosity and magnetic diffusivity parameters are different from one ensemble member to another.

Recent studies show that instead of solving coupled MHD systems in primitive variables, using instead Elsässer variables can provide a decoupled stable MHD simulation algorithm, [1, 14, 34, 35, 42, 43]. Defining $\mathbf{v}_j := \mathbf{u}_j + \sqrt{s}\mathbf{B}_j$, $\mathbf{w}_j := \mathbf{u}_j - \sqrt{s}\mathbf{B}_j$, $\mathbf{f}_{1,j} := \mathbf{f}_j + \sqrt{s}\nabla \times \mathbf{g}_j$, $\mathbf{f}_{2,j} := \mathbf{f}_j - \sqrt{s}\nabla \times \mathbf{g}_j$, $q_j := p_j + \sqrt{s}\lambda_j$ and $r_j := p_j - \sqrt{s}\lambda_j$ produces the Elsässer variable formulation of the ensemble systems:

$$\mathbf{v}_{j,t} + \mathbf{w}_j \cdot \nabla \mathbf{v}_j - \frac{\nu_j + \nu_{m,j}}{2} \Delta \mathbf{v}_j - \frac{\nu_j - \nu_{m,j}}{2} \Delta \mathbf{w}_j + \nabla q_j = \mathbf{f}_{1,j}, \quad (1.7)$$

$$\mathbf{w}_{j,t} + \mathbf{v}_j \cdot \nabla \mathbf{w}_j - \frac{\nu_j + \nu_{m,j}}{2} \Delta \mathbf{w}_j - \frac{\nu_j - \nu_{m,j}}{2} \Delta \mathbf{v}_j + \nabla r_j = \mathbf{f}_{2,j}, \quad (1.8)$$

$$\nabla \cdot \mathbf{v}_j = \nabla \cdot \mathbf{w}_j = 0, \quad (1.9)$$

together with the initial and boundary conditions.

To reduce the immense computational cost for the above ensemble system, we propose a decoupled scheme together with the breakthrough idea Jiang and Layton from [20]. Thus, we consider a uniform time-step size Δt and let $t_n = n\Delta t$ for $n = 0, 1, \dots$, (suppress the spatial discretization momentarily), then computing the J solutions independently, takes the following form:

Step 1: For $j = 1, \dots, J$,

$$\begin{aligned} \frac{\mathbf{v}_j^{n+1}}{\Delta t} + \langle \mathbf{w} \rangle^n \cdot \nabla \mathbf{v}_j^{n+1} - \frac{\bar{\nu} + \bar{\nu}_m}{2} \Delta \mathbf{v}_j^{n+1} - \nabla \cdot \left(2\nu_T(\mathbf{w}', t^n) \nabla \mathbf{v}_j^{n+1} \right) + \nabla q_j^{n+1} \\ = \mathbf{f}_{1,j}(t^{n+1}) + \frac{\mathbf{v}_j^n}{\Delta t} - \mathbf{w}_j^n \cdot \nabla \mathbf{v}_j^n + \frac{\nu_j' + \nu_{m,j}'}{2} \Delta \mathbf{v}_j^n + \frac{\nu_j - \nu_{m,j}}{2} \Delta \mathbf{w}_j^n, \end{aligned} \quad (1.10)$$

$$\nabla \cdot \mathbf{v}_j^{n+1} = 0. \quad (1.11)$$

Step 2: For $j = 1, \dots, J$,

$$\begin{aligned} \frac{\mathbf{w}_j^{n+1}}{\Delta t} + \langle \mathbf{v} \rangle^n \cdot \nabla \mathbf{w}_j^{n+1} - \frac{\bar{\nu} + \bar{\nu}_m}{2} \Delta \mathbf{w}_j^{n+1} - \nabla \cdot \left(2\nu_T(\mathbf{v}', t^n) \nabla \mathbf{w}_j^{n+1} \right) + \nabla r_j^{n+1} \\ = \mathbf{f}_{2,j}(t^{n+1}) + \frac{\mathbf{w}_j^n}{\Delta t} - \mathbf{v}_j^n \cdot \nabla \mathbf{w}_j^n + \frac{\nu_j' + \nu_{m,j}'}{2} \Delta \mathbf{w}_j^n + \frac{\nu_j - \nu_{m,j}}{2} \Delta \mathbf{v}_j^n, \end{aligned} \quad (1.12)$$

$$\nabla \cdot \mathbf{w}_j^{n+1} = 0. \quad (1.13)$$

Here, \mathbf{v}_j^n , \mathbf{w}_j^n , q_j^n , and r_j^n denote approximations of $\mathbf{v}_j(\cdot, t^n)$, $\mathbf{w}_j(\cdot, t^n)$, $q_j(\cdot, t^n)$, and $r_j(\cdot, t^n)$, respectively. The ensemble mean and fluctuation about the mean are defined as follows:

$$\begin{aligned} \langle \mathbf{z} \rangle^n &:= \frac{1}{J} \sum_{j=1}^J \mathbf{z}_j^n, \quad \mathbf{z}_j^n := \mathbf{z}_j^n - \langle \mathbf{z} \rangle^n, \\ \bar{\nu} &:= \frac{1}{J} \sum_{j=1}^J \nu_j, \quad \nu_j' := \nu_j - \bar{\nu}, \text{ and} \\ \bar{\nu}_m &:= \frac{1}{J} \sum_{j=1}^J \nu_{j,m}, \quad \nu_{j,m}' := \nu_{j,m} - \bar{\nu}_m. \end{aligned}$$

The eddy viscosity term, which is $O(\Delta t)$, is defined using mixing length phenomenology, following [21], and is given by $\nu_T(\mathbf{z}', t^n) := \mu \Delta t (l_z^n)^2$, where μ is a tuning parameter, $l_z^n = \max_j |\mathbf{z}_j^n|$ is a scalar quantity, and $|\cdot|$ denotes length of a vector.

At each time-step, the above identical subproblems can be solved *simultaneously* and they each share the exact same system matrix (which is independent of j). Hence, to solve for the next time-step, one solves the following system of equations of the form $A[\mathbf{x}_1|\mathbf{x}_2|\cdots|\mathbf{x}_J] = [\mathbf{b}_1|\mathbf{b}_2|\cdots|\mathbf{b}_J]$. Therefore, a massive amount of computer memory is saved and system matrix assembly and factorization/preconditioner are needed only once per time-step. Moreover, the algorithm can take advantage of block linear solvers [24]. This idea in [20] has been implemented for the solution of the heat equation with uncertain temperature-dependent conductivity [8], Navier-Stokes simulations [17, 18, 21, 38], magnetohydrodynamics [23, 35], parameterized flow problems [12, 30], and turbulence modeling [19]. Using a finite element spatial discretization, we investigate the proposed decoupled ensemble scheme (1.10)-(1.13) in a fully discrete setting. The efficient ensemble scheme is stable and convergent without any time-step restriction, and handles, uncertainties in all input data. The rest of the paper is organized as follows: To follow a smooth analysis, we provide necessary notations and mathematical preliminaries in Section 2. In Section 3, we present and analyze a fully discrete and decoupled algorithm corresponding to (1.10)-(1.13), and prove stability and convergent theorems for it. To support the theoretical analysis, we compute the convergence rates, check the energy stability of the scheme, and test the scheme on benchmark problems in Section 4. Finally, conclusions and future research avenues are given in Section 5.

2. Notation and preliminaries. Let $\Omega \subset \mathbb{R}^d$ ($d = 2, 3$) be a convex polygonal or polyhedral domain with boundary $\partial\Omega$. The usual $L^2(\Omega)$ norm and inner product are denoted by $\|\cdot\|$ and (\cdot, \cdot) , respectively. Similarly, the $L^p(\Omega)$ norms and the Sobolev $W_p^k(\Omega)$ norms are $\|\cdot\|_{L^p}$ and $\|\cdot\|_{W_p^k}$, respectively for $k \in \mathbb{N}$, $1 \leq p \leq \infty$. The Sobolev space $W_2^k(\Omega)$ is represented by $H^k(\Omega)$ with norm $\|\cdot\|_k$. The vector-valued spaces are

$$\mathbf{L}^p(\Omega) = (L^p(\Omega))^d, \text{ and } \mathbf{H}^k(\Omega) = (H^k(\Omega))^d.$$

For \mathbf{X} being a normed function space in Ω , $L^p(0, T; \mathbf{X})$ is the space of all functions defined on $(0, T] \times \Omega$ for which the following norm

$$\|\mathbf{u}\|_{L^p(0, T; \mathbf{X})} = \left(\int_0^T \|\mathbf{u}\|_{\mathbf{X}}^p dt \right)^{\frac{1}{p}}, \quad p \in [1, \infty)$$

is finite. For $p = \infty$, the usual modification is used in the definition of this space. The natural function spaces for our problem are

$$\begin{aligned} \mathbf{X} &:= \mathbf{H}_0^1(\Omega) = \{\mathbf{v} \in \mathbf{L}^p(\Omega) : \nabla \mathbf{v} \in L^2(\Omega)^{d \times d}, \mathbf{v} = \mathbf{0} \text{ on } \partial\Omega\}, \\ Q &:= L_0^2(\Omega) = \{q \in L^2(\Omega) : \int_{\Omega} q \, d\mathbf{x} = 0\}. \end{aligned}$$

Recall the Poincaré inequality holds in \mathbf{X} : There exists C depending only on Ω satisfying for all $\varphi \in \mathbf{X}$,

$$\|\varphi\| \leq C \|\nabla \varphi\|.$$

The divergence-free velocity space is given by

$$\mathbf{V} := \{\mathbf{v} \in \mathbf{X} : (\nabla \cdot \mathbf{v}, q) = 0, \forall q \in Q\}.$$

We define the trilinear form $b : \mathbf{X} \times \mathbf{X} \times \mathbf{X} \rightarrow \mathbb{R}$ by

$$b(\mathbf{u}, \mathbf{v}, \mathbf{w}) := (\mathbf{u} \cdot \nabla \mathbf{v}, \mathbf{w}),$$

and recall from [10] that $b(\mathbf{u}, \mathbf{v}, \mathbf{v}) = 0$ if $\mathbf{u} \in \mathbf{V}$, and

$$|b(\mathbf{u}, \mathbf{v}, \mathbf{w})| \leq C(\Omega) \|\nabla \mathbf{u}\| \|\nabla \mathbf{v}\| \|\nabla \mathbf{w}\|, \text{ for any } \mathbf{u}, \mathbf{v}, \mathbf{w} \in \mathbf{X}. \quad (2.1)$$

The conforming finite element spaces are denoted by $\mathbf{X}_h \subset \mathbf{X}$ and $Q_h \subset Q$, and we assume a regular triangulation $\tau_h(\Omega)$, where h is the maximum triangle diameter. We assume that (\mathbf{X}_h, Q_h) satisfies the usual discrete *inf-sup* condition

$$\inf_{q_h \in Q_h} \sup_{\mathbf{v}_h \in \mathbf{X}_h} \frac{(q_h, \nabla \cdot \mathbf{v}_h)}{\|q_h\| \|\nabla \mathbf{v}_h\|} \geq \beta > 0, \quad (2.2)$$

where β is independent of h . The space of discretely divergence-free functions is defined as

$$\mathbf{V}_h := \{\mathbf{v}_h \in \mathbf{X}_h : (\nabla \cdot \mathbf{v}_h, q_h) = 0, \quad \forall q_h \in Q_h\}.$$

For simplicity of our analysis, we will use the Scott-Vogelius (SV) finite element pair $(\mathbf{X}_h, Q_h) = ((P_k)^d, P_{k-1}^{disc})$, which satisfies the *inf-sup* condition under certain conditions, such as when the mesh is created as a barycenter refinement of a regular mesh and the polynomial degree $k \geq d$ [2, 45]. Our analysis can be extended without difficulty to any *inf-sup* stable element choice, although with minor additional technical detail.

We have the following approximation properties in (\mathbf{X}_h, Q_h) : [5]

$$\inf_{\mathbf{v}_h \in \mathbf{X}_h} \|\mathbf{u} - \mathbf{v}_h\| \leq Ch^{k+1} |\mathbf{u}|_{k+1}, \quad \mathbf{u} \in \mathbf{H}^{k+1}(\Omega), \quad (2.3)$$

$$\inf_{\mathbf{v}_h \in \mathbf{X}_h} \|\nabla(\mathbf{u} - \mathbf{v}_h)\| \leq Ch^k |\mathbf{u}|_{k+1}, \quad \mathbf{u} \in \mathbf{H}^{k+1}(\Omega), \quad (2.4)$$

$$\inf_{q_h \in Q_h} \|p - q_h\| \leq Ch^k |p|_k, \quad p \in H^k(\Omega), \quad (2.5)$$

where $|\cdot|_r$ denotes the H^r or \mathbf{H}^r seminorm.

We will assume the mesh is sufficiently regular for the inverse inequality to hold, and with this and the LBB assumption, we have approximation properties

$$\|\nabla(\mathbf{u} - P_{\mathbf{V}_h}^{L^2}(\mathbf{u}))\| \leq Ch^k |\mathbf{u}|_{k+1}, \quad \mathbf{u} \in \mathbf{H}^{k+1}(\Omega), \quad (2.6)$$

$$\inf_{\mathbf{v}_h \in \mathbf{V}_h} \|\nabla(\mathbf{u} - \mathbf{v}_h)\| \leq Ch^k |\mathbf{u}|_{k+1}, \quad \mathbf{u} \in \mathbf{H}^{k+1}(\Omega), \quad (2.7)$$

where $P_{\mathbf{V}_h}^{L^2}(\mathbf{u})$ is the L^2 projection of \mathbf{u} into \mathbf{V}_h .

The following lemma for the discrete Grönwall inequality was given in [15].

Lemma 2.1. *Let Δt , \mathcal{D} , a_n , b_n , c_n , d_n be non-negative numbers for $n = 1, \dots, M$ such that*

$$a_M + \Delta t \sum_{n=1}^M b_n \leq \Delta t \sum_{n=1}^{M-1} d_n a_n + \Delta t \sum_{n=1}^M c_n + \mathcal{D} \quad \text{for } M \in \mathbb{N},$$

then for all $\Delta t > 0$,

$$a_M + \Delta t \sum_{n=1}^M b_n \leq \exp\left(\Delta t \sum_{n=1}^{M-1} d_n\right) \left(\Delta t \sum_{n=1}^M c_n + \mathcal{D}\right) \quad \text{for } M \in \mathbb{N}.$$

3. Fully discrete scheme and analysis. Now we present and analyze an efficient, fully discrete, and decoupled time-stepping scheme for computing MHD flow ensembles. The scheme is

defined below.

Algorithm 1: Fully discrete and decoupled ensemble scheme

Given time-step $\Delta t > 0$, end time $T > 0$, initial conditions $\mathbf{v}_j^0, \mathbf{w}_j^0 \in \mathbf{V}_h$ and $\mathbf{f}_{1,j}, \mathbf{f}_{2,j} \in L^\infty(0, T; \mathbf{H}^{-1}(\Omega))$ for $j = 1, 2, \dots, J$. Set $M = T/\Delta t$ and for $n = 1, \dots, M-1$, compute:
Find $\mathbf{v}_{j,h}^{n+1} \in \mathbf{V}_h$ satisfying, for all $\chi_{j,h} \in \mathbf{V}_h$:

$$\begin{aligned} & \left(\frac{\mathbf{v}_{j,h}^{n+1} - \mathbf{v}_{j,h}^n}{\Delta t}, \chi_{j,h} \right) + b \left(\langle \mathbf{w}_h \rangle^n, \mathbf{v}_{j,h}^{n+1}, \chi_{j,h} \right) + \frac{\bar{\nu} + \bar{\nu}_m}{2} \left(\nabla \mathbf{v}_{j,h}^{n+1}, \nabla \chi_{j,h} \right) \\ & + \left(2\nu_T(\mathbf{w}'_h, t^n) \nabla \mathbf{v}_{j,h}^{n+1}, \nabla \chi_{j,h} \right) = \left(\mathbf{f}_{1,j}(t^{n+1}), \chi_{j,h} \right) - b \left(\mathbf{w}'_{j,h}, \mathbf{v}_{j,h}^n, \chi_{j,h} \right) \\ & - \frac{\nu_j - \nu_{m,j}}{2} \left(\nabla \mathbf{w}_{j,h}^n, \nabla \chi_{j,h} \right) - \frac{\nu'_j + \nu'_{m,j}}{2} \left(\nabla \mathbf{v}_{j,h}^n, \nabla \chi_{j,h} \right). \end{aligned} \quad (3.1)$$

Find $\mathbf{w}_{j,h}^{n+1} \in \mathbf{V}_h$ satisfying, for all $\mathbf{l}_{j,h} \in \mathbf{V}_h$:

$$\begin{aligned} & \left(\frac{\mathbf{w}_{j,h}^{n+1} - \mathbf{w}_{j,h}^n}{\Delta t}, \mathbf{l}_{j,h} \right) + b \left(\langle \mathbf{v}_h \rangle^n, \mathbf{w}_{j,h}^{n+1}, \mathbf{l}_{j,h} \right) + \frac{\bar{\nu} + \bar{\nu}_m}{2} \left(\nabla \mathbf{w}_{j,h}^{n+1}, \nabla \mathbf{l}_{j,h} \right) \\ & + \left(2\nu_T(\mathbf{v}'_h, t^n) \nabla \mathbf{w}_{j,h}^{n+1}, \nabla \mathbf{l}_{j,h} \right) = \left(\mathbf{f}_{2,j}(t^{n+1}), \mathbf{l}_{j,h} \right) - b \left(\mathbf{v}'_{j,h}, \mathbf{w}_{j,h}^n, \mathbf{l}_{j,h} \right) \\ & - \frac{\nu_j - \nu_{m,j}}{2} \left(\nabla \mathbf{v}_{j,h}^n, \nabla \mathbf{l}_{j,h} \right) - \frac{\nu'_j + \nu'_{m,j}}{2} \left(\nabla \mathbf{w}_{j,h}^n, \nabla \mathbf{l}_{j,h} \right). \end{aligned} \quad (3.2)$$

3.1. Stability analysis. We now prove stability and well-posedness for the Algorithm 1. To simplify the notation, denote $\alpha_j := \bar{\nu} + \bar{\nu}_m - |\nu_j - \nu_{m,j}| - |\nu'_j + \nu'_{m,j}|$, for $j = 1, 2, \dots, J$.

Theorem 3.1. Suppose $\mathbf{f}_{1,j}, \mathbf{f}_{2,j} \in L^\infty(0, T; \mathbf{H}^{-1}(\Omega))$, and $\mathbf{v}_{j,h}^0, \mathbf{w}_{j,h}^0 \in \mathbf{H}^1(\Omega)$, then the solutions to the Algorithm 1 are stable: For any $\Delta t > 0$, if $\alpha_j > 0$, and $\mu > \frac{1}{2}$

$$\begin{aligned} \|\mathbf{v}_{j,h}^M\|^2 + \|\mathbf{w}_{j,h}^M\|^2 + \frac{\bar{\nu} + \bar{\nu}_m}{2} \Delta t \left(\|\nabla \mathbf{v}_{j,h}^M\|^2 + \|\nabla \mathbf{w}_{j,h}^M\|^2 \right) + \frac{\alpha_j \Delta t}{2} \sum_{n=0}^{M-1} \left(\|\nabla \mathbf{v}_{j,h}^n\|^2 + \|\nabla \mathbf{w}_{j,h}^n\|^2 \right) \\ \leq \|\mathbf{v}_{j,h}^0\|^2 + \|\mathbf{w}_{j,h}^0\|^2 + \frac{\bar{\nu} + \bar{\nu}_m}{2} \Delta t \left(\|\nabla \mathbf{v}_{j,h}^0\|^2 + \|\nabla \mathbf{w}_{j,h}^0\|^2 \right) \\ + \frac{2\Delta t}{\alpha_j} \sum_{n=0}^{M-1} \left(\|\mathbf{f}_{1,j}(t^{n+1})\|_{-1}^2 + \|\mathbf{f}_{2,j}(t^{n+1})\|_{-1}^2 \right). \end{aligned}$$

Proof. Choose $\chi_{j,h} = \mathbf{v}_{j,h}^{n+1}$ and $\mathbf{l}_{j,h} = \mathbf{w}_{j,h}^{n+1}$ in (3.1)-(3.2) to obtain

$$\begin{aligned} & \left(\frac{\mathbf{v}_{j,h}^{n+1} - \mathbf{v}_{j,h}^n}{\Delta t}, \mathbf{v}_{j,h}^{n+1} \right) + \left(\mathbf{w}'_{j,h} \cdot \nabla \mathbf{v}_{j,h}^n, \mathbf{v}_{j,h}^{n+1} \right) + \frac{\bar{\nu} + \bar{\nu}_m}{2} \|\nabla \mathbf{v}_{j,h}^{n+1}\|^2 + \left(2\nu_T(\mathbf{w}'_h, t^n) \nabla \mathbf{v}_{j,h}^{n+1}, \nabla \mathbf{v}_{j,h}^{n+1} \right) \\ & = \left(\mathbf{f}_{1,j}(t^{n+1}), \mathbf{v}_{j,h}^{n+1} \right) - \frac{\nu_j - \nu_{m,j}}{2} \left(\nabla \mathbf{w}_{j,h}^n, \nabla \mathbf{v}_{j,h}^{n+1} \right) - \frac{\nu'_j + \nu'_{m,j}}{2} \left(\nabla \mathbf{v}_{j,h}^n, \nabla \mathbf{v}_{j,h}^{n+1} \right), \end{aligned} \quad (3.3)$$

and

$$\begin{aligned} & \left(\frac{\mathbf{w}_{j,h}^{n+1} - \mathbf{w}_{j,h}^n}{\Delta t}, \mathbf{w}_{j,h}^{n+1} \right) + \left(\mathbf{v}'_{j,h} \cdot \nabla \mathbf{w}_{j,h}^n, \mathbf{w}_{j,h}^{n+1} \right) + \frac{\bar{\nu} + \bar{\nu}_m}{2} \|\nabla \mathbf{w}_{j,h}^{n+1}\|^2 + \left(2\nu_T(\mathbf{v}'_h, t^n) \nabla \mathbf{w}_{j,h}^{n+1}, \nabla \mathbf{w}_{j,h}^{n+1} \right) \\ & = \left(\mathbf{f}_{2,j}(t^{n+1}), \mathbf{w}_{j,h}^{n+1} \right) - \frac{\nu_j - \nu_{m,j}}{2} \left(\nabla \mathbf{v}_{j,h}^n, \nabla \mathbf{w}_{j,h}^{n+1} \right) - \frac{\nu'_j + \nu'_{m,j}}{2} \left(\nabla \mathbf{w}_{j,h}^n, \nabla \mathbf{w}_{j,h}^{n+1} \right). \end{aligned} \quad (3.4)$$

Using the polarization identity and that $(2\nu_T(\mathbf{w}'_h, t^n)\nabla\mathbf{v}_{j,h}^{n+1}, \nabla\mathbf{v}_{j,h}^{n+1}) = 2\mu\Delta t\|\mathbf{l}_{w,h}^n\nabla\mathbf{v}_{j,h}^{n+1}\|^2$, we get

$$\begin{aligned} & \frac{1}{2\Delta t} \left(\|\mathbf{v}_{j,h}^{n+1} - \mathbf{v}_{j,h}^n\|^2 + \|\mathbf{v}_{j,h}^{n+1}\|^2 - \|\mathbf{v}_{j,h}^n\|^2 \right) + \left(\mathbf{w}'_{j,h} \cdot \nabla\mathbf{v}_{j,h}^n, \mathbf{v}_{j,h}^{n+1} \right) \\ & + \frac{\bar{\nu} + \bar{\nu}_m}{2} \|\nabla\mathbf{v}_{j,h}^{n+1}\|^2 + 2\mu\Delta t\|\mathbf{l}_{w,h}^n\nabla\mathbf{v}_{j,h}^{n+1}\|^2 = \left(\mathbf{f}_{1,j}(t^{n+1}), \mathbf{v}_{j,h}^{n+1} \right) \\ & - \frac{\nu_j - \nu_{m,j}}{2} \left(\nabla\mathbf{w}_{j,h}^n, \nabla\mathbf{v}_{j,h}^{n+1} \right) - \frac{\nu'_j + \nu'_{m,j}}{2} \left(\nabla\mathbf{v}_{j,h}^n, \nabla\mathbf{v}_{j,h}^{n+1} \right), \end{aligned} \quad (3.5)$$

and

$$\begin{aligned} & \frac{1}{2\Delta t} \left(\|\mathbf{w}_{j,h}^{n+1} - \mathbf{w}_{j,h}^n\|^2 + \|\mathbf{w}_{j,h}^{n+1}\|^2 - \|\mathbf{w}_{j,h}^n\|^2 \right) + \left(\mathbf{v}'_{j,h} \cdot \nabla\mathbf{w}_{j,h}^n, \mathbf{w}_{j,h}^{n+1} \right) \\ & + \frac{\bar{\nu} + \bar{\nu}_m}{2} \|\nabla\mathbf{w}_{j,h}^{n+1}\|^2 + 2\mu\Delta t\|\mathbf{l}_{v,h}^n\nabla\mathbf{w}_{j,h}^{n+1}\|^2 = \left(\mathbf{f}_{2,j}(t^{n+1}), \mathbf{w}_{j,h}^{n+1} \right) \\ & - \frac{\nu_j - \nu_{m,j}}{2} \left(\nabla\mathbf{v}_{j,h}^n, \nabla\mathbf{w}_{j,h}^{n+1} \right) - \frac{\nu'_j + \nu'_{m,j}}{2} \left(\nabla\mathbf{w}_{j,h}^n, \nabla\mathbf{w}_{j,h}^{n+1} \right). \end{aligned} \quad (3.6)$$

Adding (3.5) and (3.6), using inequality $\|\mathbf{a} \cdot \nabla\mathbf{b}\| \leq \|\mathbf{a}\|\|\nabla\mathbf{b}\|$ in

$$\begin{aligned} \left(\mathbf{w}'_{j,h} \cdot \nabla\mathbf{v}_{j,h}^n, \mathbf{v}_{j,h}^{n+1} \right) &= - \left(\mathbf{w}'_{j,h} \cdot \nabla\mathbf{v}_{j,h}^{n+1}, \mathbf{v}_{j,h}^n \right) \\ &= \left(\mathbf{w}'_{j,h} \cdot \nabla\mathbf{v}_{j,h}^{n+1}, \mathbf{v}_{j,h}^{n+1} - \mathbf{v}_{j,h}^n \right) \\ &\leq \|\mathbf{w}'_{j,h} \cdot \nabla\mathbf{v}_{j,h}^{n+1}\| \|\mathbf{v}_{j,h}^{n+1} - \mathbf{v}_{j,h}^n\| \\ &\leq \|\mathbf{w}'_{j,h}\| \|\nabla\mathbf{v}_{j,h}^{n+1}\| \|\mathbf{v}_{j,h}^{n+1} - \mathbf{v}_{j,h}^n\| \\ &\leq \|\mathbf{l}_{w,h}^n\nabla\mathbf{v}_{j,h}^{n+1}\| \|\mathbf{v}_{j,h}^{n+1} - \mathbf{v}_{j,h}^n\|, \end{aligned}$$

and after applying the Cauchy-Schwarz inequality, reduces to

$$\begin{aligned} & \frac{1}{2\Delta t} \left(\|\mathbf{v}_{j,h}^{n+1}\|^2 - \|\mathbf{v}_{j,h}^n\|^2 + \|\mathbf{w}_{j,h}^{n+1}\|^2 - \|\mathbf{w}_{j,h}^n\|^2 + \|\mathbf{v}_{j,h}^{n+1} - \mathbf{v}_{j,h}^n\|^2 + \|\mathbf{w}_{j,h}^{n+1} - \mathbf{w}_{j,h}^n\|^2 \right) \\ & + \frac{\bar{\nu} + \bar{\nu}_m}{2} \left(\|\nabla\mathbf{v}_{j,h}^{n+1}\|^2 + \|\nabla\mathbf{w}_{j,h}^{n+1}\|^2 \right) + 2\mu\Delta t \left(\|\mathbf{l}_{w,h}^n\nabla\mathbf{v}_{j,h}^{n+1}\|^2 + \|\mathbf{l}_{v,h}^n\nabla\mathbf{w}_{j,h}^{n+1}\|^2 \right) \\ & \leq \|\mathbf{l}_{w,h}^n\nabla\mathbf{v}_{j,h}^{n+1}\| \|\mathbf{v}_{j,h}^{n+1} - \mathbf{v}_{j,h}^n\| + \|\mathbf{l}_{v,h}^n\nabla\mathbf{w}_{j,h}^{n+1}\| \|\mathbf{w}_{j,h}^{n+1} - \mathbf{w}_{j,h}^n\| \\ & + \|\mathbf{f}_{1,j}(t^{n+1})\|_{-1} \|\nabla\mathbf{v}_{j,h}^{n+1}\| + \|\mathbf{f}_{2,j}(t^{n+1})\|_{-1} \|\nabla\mathbf{w}_{j,h}^{n+1}\| \\ & + \frac{|\nu'_j + \nu'_{m,j}|}{2} \left(\|\nabla\mathbf{v}_{j,h}^{n+1}\| \|\nabla\mathbf{v}_{j,h}^n\| + \|\nabla\mathbf{w}_{j,h}^n\| \|\nabla\mathbf{w}_{j,h}^{n+1}\| \right) \\ & + \frac{|\nu_j - \nu_{m,j}|}{2} \left(\|\nabla\mathbf{v}_{j,h}^{n+1}\| \|\nabla\mathbf{w}_{j,h}^n\| + \|\nabla\mathbf{w}_{j,h}^{n+1}\| \|\nabla\mathbf{v}_{j,h}^n\| \right). \end{aligned} \quad (3.7)$$

Using Young's inequality and reducing, we have

$$\begin{aligned} & \frac{1}{2\Delta t} \left(\|\mathbf{v}_{j,h}^{n+1}\|^2 - \|\mathbf{v}_{j,h}^n\|^2 + \|\mathbf{w}_{j,h}^{n+1}\|^2 - \|\mathbf{w}_{j,h}^n\|^2 \right) + \frac{1}{4\Delta t} \left(\|\mathbf{v}_{j,h}^{n+1} - \mathbf{v}_{j,h}^n\|^2 + \|\mathbf{w}_{j,h}^{n+1} - \mathbf{w}_{j,h}^n\|^2 \right) \\ & + \frac{\bar{\nu} + \bar{\nu}_m}{4} \left(\|\nabla\mathbf{v}_{j,h}^{n+1}\|^2 + \|\nabla\mathbf{w}_{j,h}^{n+1}\|^2 \right) + (2\mu - 1)\Delta t \left(\|\mathbf{l}_{w,h}^n\nabla\mathbf{v}_{j,h}^{n+1}\|^2 + \|\mathbf{l}_{v,h}^n\nabla\mathbf{w}_{j,h}^{n+1}\|^2 \right) \\ & \leq \frac{|\nu_j - \nu_{m,j}| + |\nu'_j + \nu'_{m,j}|}{4} \left(\|\nabla\mathbf{v}_{j,h}^n\|^2 + \|\nabla\mathbf{w}_{j,h}^n\|^2 \right) \\ & + \frac{1}{\alpha_j} \left(\|\mathbf{f}_{1,j}(t^{n+1})\|_{-1}^2 + \|\mathbf{f}_{2,j}(t^{n+1})\|_{-1}^2 \right). \end{aligned} \quad (3.8)$$

Assuming $\mu > \frac{1}{2}$, and dropping non-negative terms from the left-hand-side, this reduces to

$$\begin{aligned}
& \frac{1}{2\Delta t} \left(\|\mathbf{v}_{j,h}^{n+1}\|^2 - \|\mathbf{v}_{j,h}^n\|^2 + \|\mathbf{w}_{j,h}^{n+1}\|^2 - \|\mathbf{w}_{j,h}^n\|^2 \right) \\
& + \frac{\bar{\nu} + \bar{\nu}_m}{4} \left(\|\nabla \mathbf{v}_{j,h}^{n+1}\|^2 - \|\nabla \mathbf{v}_{j,h}^n\|^2 + \|\nabla \mathbf{w}_{j,h}^{n+1}\|^2 - \|\nabla \mathbf{w}_{j,h}^n\|^2 \right) \\
& + \frac{\alpha_j}{4} (\|\nabla \mathbf{v}_{j,h}^n\|^2 + \|\nabla \mathbf{w}_{j,h}^n\|^2) \leq \frac{1}{\alpha_j} (\|\mathbf{f}_{1,j}(t^{n+1})\|_{-1}^2 + \|\mathbf{f}_{2,j}(t^{n+1})\|_{-1}^2). \quad (3.9)
\end{aligned}$$

Multiplying both sides by $2\Delta t$, and summing over time-steps $n = 0, \dots, M-1$, completes the proof.

□

Remark 3.1. *The Algorithm 1 is finite dimensional and linear at each time-step, thus the above stability implies the well-posedness of the scheme. Again, due to the linearity, the stability provides uniqueness, and uniqueness implies existence.*

3.2. Convergence. We now prove the convergence of the proposed decoupled and unconditionally stable Algorithm 1, which converges in space and time, provided that the true solution is sufficiently smooth.

Theorem 3.2. *Assume $(\mathbf{v}_j, \mathbf{w}_j, q_j, r_j)$ satisfying (1.7)-(1.9) with regularity assumptions $\mathbf{v}_j, \mathbf{w}_j \in L^\infty(0, T; \mathbf{H}^{k+1}(\Omega))$, $\mathbf{v}_{j,t}, \mathbf{w}_{j,t} \in L^\infty(0, T; \mathbf{H}^2(\Omega))$, $\mathbf{v}_{j,tt}, \mathbf{w}_{j,tt} \in L^\infty(0, T; \mathbf{L}^2(\Omega))$ for $j = 1, 2, \dots, J$, then the ensemble average solution $(\langle \mathbf{v}_h \rangle, \langle \mathbf{w}_h \rangle)$ to the Algorithm 1 converges to the true ensemble average solution: For any $\Delta t > 0$, if $\alpha_j > 0$, and $\mu > \frac{1}{2}$, one has*

$$\begin{aligned}
& \|\langle \mathbf{v} \rangle(T) - \langle \mathbf{v}_h \rangle^M\|^2 + \|\langle \mathbf{w} \rangle(T) - \langle \mathbf{w}_h \rangle^M\|^2 + \frac{\alpha_j \Delta t}{2} \sum_{n=1}^M \left(\|\nabla(\langle \mathbf{v} \rangle(t^n) - \langle \mathbf{v}_h \rangle^n)\|^2 \right. \\
& \left. + \|\nabla(\langle \mathbf{w} \rangle(t^n) - \langle \mathbf{w}_h \rangle^n)\|^2 \right) \leq C \exp \left(\frac{CT}{\alpha_j} \left(1 + \frac{\Delta t^2}{J} \right) \right) \left(\Delta t^2 + h^{2k} + h^{2k} \Delta t^2 \right. \\
& \left. + h^{2-d} \Delta t^2 + h^{2k-1} \Delta t + h^{2k+2} \right). \quad (3.10)
\end{aligned}$$

Remark 3.2. *In 3D, the predicted temporal convergence rate could be reduced to $O(\Delta t(1+h^{-1/2}))$, which is less than the optimal rate $O(\Delta t)$. This reduction happens due to the use of inverse inequality in the analysis of the stabilization term. It can be improved to $O(\Delta t)$ without using the stabilization term in the scheme, but that will incur a time-step restriction for the stability and convergence theorems.*

Proof. We start our proof by obtaining the error equations. Testing (1.7) and (1.8) with $\chi_{j,h}, \mathbf{l}_{j,h} \in \mathbf{V}_h$ at the time level t^{n+1} , the continuous variational formulations can be written as

$$\begin{aligned}
& \left(\frac{\mathbf{v}_j(t^{n+1}) - \mathbf{v}_j(t^n)}{\Delta t}, \chi_{j,h} \right) + \left(\mathbf{w}_j(t^{n+1}) \cdot \nabla \mathbf{v}_j(t^{n+1}), \chi_{j,h} \right) + \frac{\bar{\nu} + \bar{\nu}_m}{2} \left(\nabla \mathbf{v}_j(t^{n+1}), \nabla \chi_{j,h} \right) \\
& = \left(\mathbf{f}_{1,j}(t^{n+1}), \chi_{j,h} \right) - \frac{\nu'_j + \nu'_{m,j}}{2} \left(\nabla \mathbf{v}_j(t^{n+1}), \nabla \chi_{j,h} \right) - \frac{\nu_j - \nu_{m,j}}{2} \left(\nabla \mathbf{w}_j(t^n), \nabla \chi_{j,h} \right) \\
& - \frac{\nu_j - \nu_{m,j}}{2} \left(\nabla (\mathbf{w}_j(t^{n+1}) - \mathbf{w}_j(t^n)), \nabla \chi_{j,h} \right) - \left(\mathbf{v}_{j,t}(t^{n+1}) - \frac{\mathbf{v}_j(t^{n+1}) - \mathbf{v}_j(t^n)}{\Delta t}, \chi_{j,h} \right), \quad (3.11)
\end{aligned}$$

and

$$\begin{aligned}
& \left(\frac{\mathbf{w}_j(t^{n+1}) - \mathbf{w}_j(t^n)}{\Delta t}, \mathbf{l}_{j,h} \right) + \left(\mathbf{v}_j(t^{n+1}) \cdot \nabla \mathbf{w}_j(t^{n+1}), \mathbf{l}_{j,h} \right) + \frac{\bar{\nu} + \bar{\nu}_m}{2} \left(\nabla \mathbf{w}_j(t^{n+1}), \nabla \mathbf{l}_{j,h} \right) \\
& = \left(\mathbf{f}_{2,j}(t^{n+1}), \mathbf{l}_{j,h} \right) - \frac{\nu'_j + \nu'_{m,j}}{2} \left(\nabla \mathbf{w}_j(t^{n+1}), \nabla \mathbf{l}_{j,h} \right) - \frac{\nu_j - \nu_{m,j}}{2} \left(\nabla \mathbf{v}_j(t^n), \nabla \mathbf{l}_{j,h} \right) \\
& - \frac{\nu_j - \nu_{m,j}}{2} \left(\nabla (\mathbf{v}_j(t^{n+1}) - \mathbf{v}_j(t^n)), \nabla \mathbf{l}_{j,h} \right) - \left(\mathbf{w}_{j,t}(t^{n+1}) - \frac{\mathbf{w}_j(t^{n+1}) - \mathbf{w}_j(t^n)}{\Delta t}, \mathbf{l}_{j,h} \right). \quad (3.12)
\end{aligned}$$

Denote $\mathbf{e}_{\mathbf{v},j}^n := \mathbf{v}_j(t^n) - \mathbf{v}_{j,h}^n$, $\mathbf{e}_{\mathbf{w},j}^n := \mathbf{w}_j(t^n) - \mathbf{w}_{j,h}^n$. Subtracting (3.1) and (3.2) from equation (3.11) and (3.12), respectively, yields

$$\begin{aligned} & \left(\frac{\mathbf{e}_{\mathbf{v},j}^{n+1} - \mathbf{e}_{\mathbf{v},j}^n}{\Delta t}, \boldsymbol{\chi}_{j,h} \right) + \left(\langle \mathbf{e}_{\mathbf{w}} \rangle^n \cdot \nabla (\mathbf{v}_j(t^{n+1}) - \mathbf{v}_j(t^n)), \boldsymbol{\chi}_{j,h} \right) + \left(\langle \mathbf{w}_h \rangle^n \cdot \nabla \mathbf{e}_{\mathbf{v},j}^{n+1}, \boldsymbol{\chi}_{j,h} \right) \\ & + \left(\mathbf{w}_{j,h}' \cdot \nabla \mathbf{e}_{\mathbf{v},j}^n, \boldsymbol{\chi}_{j,h} \right) + \left(\mathbf{e}_{\mathbf{w},j}^n \cdot \nabla \mathbf{v}_j(t^n), \boldsymbol{\chi}_{j,h} \right) + \frac{\nu_j - \nu_{m,j}}{2} \left(\nabla \mathbf{e}_{\mathbf{w},j}^n, \nabla \boldsymbol{\chi}_{j,h} \right) \\ & + \frac{\bar{\nu} + \bar{\nu}_m}{2} \left(\nabla \mathbf{e}_{\mathbf{v},j}^{n+1}, \nabla \boldsymbol{\chi}_{j,h} \right) + \frac{\nu_j' + \nu_{m,j}'}{2} \left(\nabla \mathbf{e}_{\mathbf{v},j}^n, \nabla \boldsymbol{\chi}_{j,h} \right) - 2\mu \Delta t \left((l_{w,h}^n)^2 \nabla \mathbf{v}_j(t^{n+1}), \nabla \boldsymbol{\chi}_{j,h} \right) \\ & + 2\mu \Delta t \left((l_{w,h}^n)^2 \nabla \mathbf{e}_{\mathbf{v},j}^{n+1}, \nabla \boldsymbol{\chi}_{j,h} \right) = -G_1(t, \mathbf{v}_j, \mathbf{w}_j, \boldsymbol{\chi}_{j,h}), \end{aligned} \quad (3.13)$$

and

$$\begin{aligned} & \left(\frac{\mathbf{e}_{\mathbf{w},j}^{n+1} - \mathbf{e}_{\mathbf{w},j}^n}{\Delta t}, \mathbf{l}_{j,h} \right) + \left(\langle \mathbf{e}_{\mathbf{v}} \rangle^n \cdot \nabla (\mathbf{w}_j(t^{n+1}) - \mathbf{w}_j(t^n)), \mathbf{l}_{j,h} \right) + \left(\langle \mathbf{v}_h \rangle^n \cdot \nabla \mathbf{e}_{\mathbf{w},j}^{n+1}, \mathbf{l}_{j,h} \right) \\ & + \left(\mathbf{v}_{j,h}' \cdot \nabla \mathbf{e}_{\mathbf{w},j}^n, \mathbf{l}_{j,h} \right) + \left(\mathbf{e}_{\mathbf{v},j}^n \cdot \nabla \mathbf{w}_j(t^n), \mathbf{l}_{j,h} \right) + \frac{\nu_j - \nu_{m,j}}{2} \left(\nabla \mathbf{e}_{\mathbf{v},j}^n, \nabla \mathbf{l}_{j,h} \right) \\ & + \frac{\bar{\nu} + \bar{\nu}_m}{2} \left(\nabla \mathbf{e}_{\mathbf{w},j}^{n+1}, \nabla \mathbf{l}_{j,h} \right) + \frac{\nu_j' + \nu_{m,j}'}{2} \left(\nabla \mathbf{e}_{\mathbf{w},j}^n, \nabla \mathbf{l}_{j,h} \right) - 2\mu \Delta t \left((l_{v,h}^n)^2 \nabla \mathbf{w}_j(t^{n+1}), \nabla \mathbf{l}_{j,h} \right) \\ & + 2\mu \Delta t \left((l_{v,h}^n)^2 \nabla \mathbf{e}_{\mathbf{w},j}^{n+1}, \nabla \mathbf{l}_{j,h} \right) = -G_2(t, \mathbf{v}_j, \mathbf{w}_j, \mathbf{l}_{j,h}), \end{aligned} \quad (3.14)$$

where

$$\begin{aligned} G_1(t, \mathbf{v}_j, \mathbf{w}_j, \boldsymbol{\chi}_{j,h}) &:= \left(\mathbf{v}_{j,t}(t^{n+1}) - \frac{\mathbf{v}_j(t^{n+1}) - \mathbf{v}_j(t^n)}{\Delta t}, \boldsymbol{\chi}_{j,h} \right) + \frac{\nu_j' + \nu_{m,j}'}{2} \left(\nabla (\mathbf{v}_j(t^{n+1}) - \mathbf{v}_j(t^n)), \nabla \boldsymbol{\chi}_{j,h} \right) \\ &+ \left((\mathbf{w}_j(t^{n+1}) - \mathbf{w}_j(t^n)) \cdot \nabla \mathbf{v}_j(t^{n+1}), \boldsymbol{\chi}_{j,h} \right) + \frac{\nu_j - \nu_{m,j}}{2} \left(\nabla (\mathbf{w}_j(t^{n+1}) - \mathbf{w}_j(t^n)), \nabla \boldsymbol{\chi}_{j,h} \right) \\ &+ \left((\mathbf{w}_j(t^n) - \langle \mathbf{w}(t^n) \rangle) \cdot \nabla (\mathbf{v}_j(t^{n+1}) - \mathbf{v}_j(t^n)), \boldsymbol{\chi}_{j,h} \right), \end{aligned} \quad (3.15)$$

and

$$\begin{aligned} G_2(t, \mathbf{v}_j, \mathbf{w}_j, \mathbf{l}_{j,h}) &:= \left(\mathbf{w}_{j,t}(t^{n+1}) - \frac{\mathbf{w}_j(t^{n+1}) - \mathbf{w}_j(t^n)}{\Delta t}, \mathbf{l}_{j,h} \right) + \frac{\nu_j' + \nu_{m,j}'}{2} \left(\nabla (\mathbf{w}_j(t^{n+1}) - \mathbf{w}_j(t^n)), \nabla \mathbf{l}_{j,h} \right) \\ &+ \left((\mathbf{v}_j(t^{n+1}) - \mathbf{v}_j(t^n)) \cdot \nabla \mathbf{w}_j(t^{n+1}), \mathbf{l}_{j,h} \right) + \frac{\nu_j - \nu_{m,j}}{2} \left(\nabla (\mathbf{v}_j(t^{n+1}) - \mathbf{v}_j(t^n)), \nabla \mathbf{l}_{j,h} \right) \\ &+ \left((\mathbf{v}_j(t^n) - \langle \mathbf{v}(t^n) \rangle) \cdot \nabla (\mathbf{w}_j(t^{n+1}) - \mathbf{w}_j(t^n)), \mathbf{l}_{j,h} \right). \end{aligned} \quad (3.16)$$

Now we decompose the errors as

$$\begin{aligned} \mathbf{e}_{\mathbf{v},j}^n &:= \mathbf{v}_j(t^n) - \mathbf{v}_{j,h}^n = (\mathbf{v}_j(t^n) - \tilde{\mathbf{v}}_j^n) - (\mathbf{v}_{j,h}^n - \tilde{\mathbf{v}}_j^n) := \boldsymbol{\eta}_{\mathbf{v},j}^n - \boldsymbol{\varphi}_{j,h}^n, \\ \mathbf{e}_{\mathbf{w},j}^n &:= \mathbf{w}_j(t^n) - \mathbf{w}_{j,h}^n = (\mathbf{w}_j(t^n) - \tilde{\mathbf{w}}_j^n) - (\mathbf{w}_{j,h}^n - \tilde{\mathbf{w}}_j^n) := \boldsymbol{\eta}_{\mathbf{w},j}^n - \boldsymbol{\psi}_{j,h}^n, \end{aligned}$$

where $\tilde{\mathbf{v}}_j^n := P_{\mathbf{V}_h}^{L^2}(\mathbf{v}_j(t^n)) \in \mathbf{V}_h$ and $\tilde{\mathbf{w}}_j^n := P_{\mathbf{V}_h}^{L^2}(\mathbf{w}_j(t^n)) \in \mathbf{V}_h$ are the L^2 projections of $\mathbf{v}_j(t^n)$ and $\mathbf{w}_j(t^n)$ into \mathbf{V}_h , respectively. Note that $(\boldsymbol{\eta}_{\mathbf{v},j}^n, \mathbf{v}_{j,h}) = (\boldsymbol{\eta}_{\mathbf{w},j}^n, \mathbf{v}_{j,h}) = 0 \quad \forall \mathbf{v}_{j,h} \in \mathbf{V}_h$. Rewriting, we have for $\boldsymbol{\chi}_{j,h}, \mathbf{l}_{j,h} \in \mathbf{V}_h$

$$\begin{aligned}
& \left(\frac{\varphi_{j,h}^{n+1} - \varphi_{j,h}^n}{\Delta t}, \chi_{j,h} \right) + \left(\langle \psi_h \rangle^n \cdot \nabla (v_j(t^{n+1}) - v_j(t^n)), \chi_{j,h} \right) + \left(\langle w_h \rangle^n \cdot \nabla \varphi_{j,h}^{n+1}, \chi_{j,h} \right) \\
& + \left(w'_{j,h} \cdot \nabla \varphi_{j,h}^n, \chi_{j,h} \right) + \left(\psi_{j,h}^n \cdot \nabla v_j(t^n), \chi_{j,h} \right) + \frac{\nu_j - \nu_{m,j}}{2} \left(\nabla \psi_{j,h}^n, \nabla \chi_{j,h} \right) \\
& + \frac{\bar{\nu} + \bar{\nu}_m}{2} \left(\nabla \varphi_{j,h}^{n+1}, \nabla \chi_{j,h} \right) + \frac{\nu'_j + \nu'_{m,j}}{2} \left(\nabla \varphi_{j,h}^n, \nabla \chi_{j,h} \right) + 2\mu \Delta t \left((l_{w,h}^n)^2 \nabla \varphi_{j,h}^{n+1}, \nabla \chi_{j,h} \right) \\
& = \left(\langle \eta_w \rangle^n \cdot \nabla (v_j(t^{n+1}) - v_j(t^n)), \chi_{j,h} \right) + \left(\langle w_h \rangle^n \cdot \nabla \eta_{v,j}^{n+1}, \chi_{j,h} \right) + \left(w'_{j,h} \cdot \nabla \eta_{v,j}^n, \chi_{j,h} \right) \\
& + \left(\eta_{w,j}^n \cdot \nabla v_j(t^n), \chi_{j,h} \right) + \frac{\nu_j - \nu_{m,j}}{2} \left(\nabla \eta_{w,j}^n, \nabla \chi_{j,h} \right) + \frac{\bar{\nu} + \bar{\nu}_m}{2} \left(\nabla \eta_{v,j}^{n+1}, \nabla \chi_{j,h} \right) \\
& + \frac{\nu'_j + \nu'_{m,j}}{2} \left(\nabla \eta_{v,j}^n, \nabla \chi_{j,h} \right) + 2\mu \Delta t \left((l_{w,h}^n)^2 \nabla v_j(t^{n+1}), \nabla \chi_{j,h} \right) \\
& + 2\mu \Delta t \left((l_{w,h}^n)^2 \nabla \eta_{v,j}^{n+1}, \nabla \chi_{j,h} \right) - G_1(t, v_j, w_j, \chi_{j,h}), \quad (3.17)
\end{aligned}$$

and

$$\begin{aligned}
& \left(\frac{\psi_{j,h}^{n+1} - \psi_{j,h}^n}{\Delta t}, l_{j,h} \right) + \left(\langle \varphi_h \rangle^n \cdot \nabla (w_j(t^{n+1}) - w_j(t^n)), l_{j,h} \right) + \left(\langle v_h \rangle^n \cdot \nabla \psi_{j,h}^{n+1}, l_{j,h} \right) \\
& + \left(\varphi'_{j,h} \cdot \nabla \psi_{j,h}^n, l_{j,h} \right) + \left(\varphi_{j,h}^n \cdot \nabla w_j(t^n), l_{j,h} \right) + \frac{\nu_j - \nu_{m,j}}{2} \left(\nabla \varphi_{j,h}^n, \nabla l_{j,h} \right) \\
& + \frac{\bar{\nu} + \bar{\nu}_m}{2} \left(\nabla \psi_{j,h}^{n+1}, \nabla l_{j,h} \right) + \frac{\nu'_j + \nu'_{m,j}}{2} \left(\nabla \psi_{j,h}^n, \nabla l_{j,h} \right) + 2\mu \Delta t \left((l_{v,h}^n)^2 \nabla \psi_{j,h}^{n+1}, \nabla l_{j,h} \right) \\
& = \left(\langle \eta_v \rangle^n \cdot \nabla (w_j(t^{n+1}) - w_j(t^n)), l_{j,h} \right) + \left(\langle v_h \rangle^n \cdot \nabla \eta_{w,j}^{n+1}, l_{j,h} \right) + \left(v'_{j,h} \cdot \nabla \eta_{w,j}^n, l_{j,h} \right) \\
& + \left(\eta_{v,j}^n \cdot \nabla w_j(t^n), l_{j,h} \right) + \frac{\nu_j - \nu_{m,j}}{2} \left(\nabla \eta_{v,j}^n, \nabla l_{j,h} \right) + \frac{\bar{\nu} + \bar{\nu}_m}{2} \left(\nabla \eta_{w,j}^{n+1}, \nabla l_{j,h} \right) \\
& + \frac{\nu'_j + \nu'_{m,j}}{2} \left(\nabla \eta_{w,j}^n, \nabla l_{j,h} \right) + 2\mu \Delta t \left((l_{v,h}^n)^2 \nabla w_j(t^{n+1}), \nabla l_{j,h} \right) \\
& + 2\mu \Delta t \left((l_{v,h}^n)^2 \nabla \eta_{w,j}^{n+1}, \nabla l_{j,h} \right) - G_2(t, v_j, w_j, l_{j,h}). \quad (3.18)
\end{aligned}$$

Choose $\chi_{j,h} = \varphi_{j,h}^{n+1}$, $l_{j,h} = \psi_{j,h}^{n+1}$, and use the polarization identity in (3.17) and (3.18), to obtain

$$\begin{aligned}
& \frac{1}{2\Delta t} \left(\|\varphi_{j,h}^{n+1}\|^2 - \|\varphi_{j,h}^n\|^2 + \|\varphi_{j,h}^{n+1} - \varphi_{j,h}^n\|^2 \right) + \frac{\bar{\nu} + \bar{\nu}_m}{2} \|\nabla \varphi_{j,h}^{n+1}\|^2 + 2\mu \Delta t \|l_{w,h}^n \nabla \varphi_{j,h}^{n+1}\|^2 \\
& \leq \frac{|\nu_j - \nu_{m,j}|}{2} \left| \left(\nabla \psi_{j,h}^n, \nabla \varphi_{j,h}^{n+1} \right) \right| + \frac{|\nu'_j + \nu'_{m,j}|}{2} \left| \left(\nabla \varphi_{j,h}^n, \nabla \varphi_{j,h}^{n+1} \right) \right| + \frac{|\nu_j - \nu_{m,j}|}{2} \left| \left(\nabla \eta_{w,j}^n, \nabla \varphi_{j,h}^{n+1} \right) \right| \\
& + \frac{\bar{\nu} + \bar{\nu}_m}{2} \left| \left(\nabla \eta_{v,j}^{n+1}, \nabla \varphi_{j,h}^{n+1} \right) \right| + \frac{|\nu'_j + \nu'_{m,j}|}{2} \left| \left(\nabla \eta_{v,j}^n, \nabla \varphi_{j,h}^{n+1} \right) \right| + \left| \left(w'_{j,h} \cdot \nabla \varphi_{j,h}^n, \varphi_{j,h}^{n+1} \right) \right| \\
& + 2\mu \Delta t \left| \left((l_{w,h}^n)^2 \nabla v_j(t^{n+1}), \nabla \varphi_{j,h}^{n+1} \right) \right| + 2\mu \Delta t \left| \left((l_{w,h}^n)^2 \nabla \eta_{v,j}^{n+1}, \nabla \varphi_{j,h}^{n+1} \right) \right| \\
& + \left| \left(\langle \psi_h \rangle^n \cdot \nabla (v_j(t^{n+1}) - v_j(t^n)), \varphi_{j,h}^{n+1} \right) \right| + \left| \left(\psi_{j,h}^n \cdot \nabla v_j(t^n), \varphi_{j,h}^{n+1} \right) \right| \\
& + \left| \left(\langle \eta_w \rangle^n \cdot \nabla (v_j(t^{n+1}) - v_j(t^n)), \varphi_{j,h}^{n+1} \right) \right| + \left| \left(\langle w_h \rangle^n \cdot \nabla \eta_{v,j}^{n+1}, \varphi_{j,h}^{n+1} \right) \right| \\
& + \left| \left(w'_{j,h} \cdot \nabla \eta_{v,j}^n, \varphi_{j,h}^{n+1} \right) \right| + \left| \left(\eta_{w,j}^n \cdot \nabla v_j(t^n), \varphi_{j,h}^{n+1} \right) \right| + \left| G_1(t, v_j, w_j, \varphi_{j,h}^{n+1}) \right|, \quad (3.19)
\end{aligned}$$

and

$$\begin{aligned}
& \frac{1}{2\Delta t} \left(\|\psi_{j,h}^{n+1}\|^2 - \|\psi_{j,h}^n\|^2 + \|\psi_{j,h}^{n+1} - \psi_{j,h}^n\|^2 \right) + \frac{\bar{\nu} + \bar{\nu}_m}{2} \|\nabla \psi_{j,h}^{n+1}\|^2 + 2\mu\Delta t \|l_{v,h}^n \nabla \psi_{j,h}^{n+1}\|^2 \\
& \leq \frac{|\nu_j - \nu_{m,j}|}{2} \left| \left(\nabla \varphi_{j,h}^n, \nabla \psi_{j,h}^{n+1} \right) \right| + \frac{|\nu'_j + \nu'_{m,j}|}{2} \left| \left(\nabla \psi_{j,h}^n, \nabla \psi_{j,h}^{n+1} \right) \right| + \frac{|\nu_j - \nu_{m,j}|}{2} \left| \left(\nabla \eta_{v,j}^n, \nabla \psi_{j,h}^{n+1} \right) \right| \\
& + \frac{\bar{\nu} + \bar{\nu}_m}{2} \left| \left(\nabla \eta_{w,j}^{n+1}, \nabla \psi_{j,h}^{n+1} \right) \right| + \frac{|\nu'_j + \nu'_{m,j}|}{2} \left| \left(\nabla \eta_{w,j}^n, \nabla \psi_{j,h}^{n+1} \right) \right| + \left| \left(\mathbf{v}_{j,h}'^n \cdot \nabla \psi_{j,h}^n, \psi_{j,h}^{n+1} \right) \right| \\
& + 2\mu\Delta t \left| \left((l_{v,h}^n)^2 \nabla \mathbf{w}_j(t^{n+1}), \nabla \psi_{j,h}^{n+1} \right) \right| + 2\mu\Delta t \left| \left((l_{v,h}^n)^2 \nabla \eta_{w,j}^{n+1}, \nabla \psi_{j,h}^{n+1} \right) \right| \\
& + \left| \left(\langle \varphi_h \rangle^n \cdot \nabla (\mathbf{w}_j(t^{n+1}) - \mathbf{w}_j(t^n)), \psi_{j,h}^{n+1} \right) \right| + \left| \left(\varphi_{j,h}^n \cdot \nabla \mathbf{w}_j(t^n), \psi_{j,h}^{n+1} \right) \right| \\
& + \left| \left(\langle \eta_v \rangle^n \cdot \nabla (\mathbf{w}_j(t^{n+1}) - \mathbf{w}_j(t^n)), \psi_{j,h}^{n+1} \right) \right| + \left| \left(\langle \mathbf{v}_h \rangle^n \cdot \nabla \eta_{w,j}^{n+1}, \psi_{j,h}^{n+1} \right) \right| \\
& + \left| \left(\mathbf{v}_{j,h}'^n \cdot \nabla \eta_{w,j}^n, \psi_{j,h}^{n+1} \right) \right| + \left| \left(\eta_{v,j}^n \cdot \nabla \mathbf{w}_j(t^n), \psi_{j,h}^{n+1} \right) \right| + \left| G_2(t, \mathbf{v}_j, \mathbf{w}_j, \psi_{j,h}^{n+1}) \right|. \tag{3.20}
\end{aligned}$$

Now, turn our attention to finding bounds on the right side terms of (3.19) (the estimates on terms in (3.20) are similar). Applying Cauchy-Schwarz Young's inequalities on the first five terms results in

$$\begin{aligned}
& \frac{|\nu_j - \nu_{m,j}|}{2} \left| \left(\nabla \psi_{j,h}^n, \nabla \varphi_{j,h}^{n+1} \right) \right| \leq \frac{|\nu_j - \nu_{m,j}|}{4} \left(\|\nabla \varphi_{j,h}^{n+1}\|^2 + \|\nabla \psi_{j,h}^n\|^2 \right), \\
& \frac{|\nu'_j + \nu'_{m,j}|}{2} \left| \left(\nabla \varphi_{j,h}^n, \nabla \varphi_{j,h}^{n+1} \right) \right| \leq \frac{|\nu'_j + \nu'_{m,j}|}{4} \left(\|\nabla \varphi_{j,h}^{n+1}\|^2 + \|\nabla \varphi_{j,h}^n\|^2 \right), \\
& \frac{|\nu_j - \nu_{m,j}|}{2} \left| \left(\nabla \eta_{w,j}^n, \nabla \varphi_{j,h}^{n+1} \right) \right| \leq \frac{\alpha_j}{44} \|\nabla \varphi_{j,h}^{n+1}\|^2 + \frac{11(\nu_j - \nu_{m,j})^2}{4\alpha_j} \|\nabla \eta_{w,j}^n\|^2, \\
& \frac{\bar{\nu} + \bar{\nu}_m}{2} \left| \left(\nabla \eta_{v,j}^{n+1}, \nabla \varphi_{j,h}^{n+1} \right) \right| \leq \frac{\alpha_j}{44} \|\nabla \varphi_{j,h}^{n+1}\|^2 + \frac{11(\bar{\nu} + \bar{\nu}_m)^2}{4\alpha_j} \|\nabla \eta_{v,j}^{n+1}\|^2, \\
& \frac{|\nu'_j + \nu'_{m,j}|}{2} \left| \left(\nabla \eta_{v,j}^n, \nabla \varphi_{j,h}^{n+1} \right) \right| \leq \frac{\alpha_j}{44} \|\nabla \varphi_{j,h}^{n+1}\|^2 + \frac{11(\nu'_j + \nu'_{m,j})^2}{4\alpha_j} \|\nabla \eta_{v,j}^n\|^2.
\end{aligned}$$

For the first nonlinear term, rearranging and applying Cauchy-Schwarz and Young's inequalities yields

$$\begin{aligned}
& \left| \left(\mathbf{w}_{j,h}'^n \cdot \nabla \varphi_{j,h}^n, \varphi_{j,h}^{n+1} \right) \right| = \left| \left(\mathbf{w}_{j,h}'^n \cdot \nabla \varphi_{j,h}^{n+1}, \varphi_{j,h}^n \right) \right| = \left| \left(\mathbf{w}_{j,h}'^n \cdot \nabla \varphi_{j,h}^{n+1}, \varphi_{j,h}^{n+1} - \varphi_{j,h}^n \right) \right| \\
& \leq \|\mathbf{w}_{j,h}'^n \cdot \nabla \varphi_{j,h}^{n+1}\| \|\varphi_{j,h}^{n+1} - \varphi_{j,h}^n\| \\
& \leq \|l_{w,h}^n \nabla \varphi_{j,h}^{n+1}\| \|\varphi_{j,h}^{n+1} - \varphi_{j,h}^n\| \\
& \leq \frac{1}{4\Delta t} \|\varphi_{j,h}^{n+1} - \varphi_{j,h}^n\|^2 + \Delta t \|l_{w,h}^n \nabla \varphi_{j,h}^{n+1}\|^2.
\end{aligned}$$

For the second nonlinear term, we apply Hölder's inequality and the regularity assumptions of the true solution to get

$$\begin{aligned}
2\mu\Delta t \left| \left((l_{w,h}^n)^2 \nabla \mathbf{v}_j(t^{n+1}), \nabla \varphi_{j,h}^{n+1} \right) \right| & \leq C\mu\Delta t \|\nabla \mathbf{v}_j(t^{n+1})\|_{L^\infty} \|l_{w,h}^n\|_{L^4}^2 \|\nabla \varphi_{j,h}^{n+1}\| \\
& \leq \frac{\alpha_j}{44} \|\nabla \varphi_{j,h}^{n+1}\|^2 + C \frac{\mu^2 \Delta t^2}{\alpha_j} \|l_{w,h}^n\|_{L^4}^4.
\end{aligned}$$

For the third nonlinear term, we rearrange, and apply Cauchy-Schwarz and Young's inequalities assuming $\mu > 1/2$ to obtain

$$\begin{aligned}
2\mu\Delta t \left| \left((l_{w,h}^n)^2 \nabla \eta_{v,j}^{n+1}, \nabla \varphi_{j,h}^{n+1} \right) \right| & = 2\mu\Delta t \left(l_{w,h}^n \nabla \eta_{v,j}^{n+1}, l_{w,h}^n \nabla \varphi_{j,h}^{n+1} \right) \\
& \leq 2\mu\Delta t \|l_{w,h}^n \nabla \eta_{v,j}^{n+1}\| \|l_{w,h}^n \nabla \varphi_{j,h}^{n+1}\| \\
& \leq \frac{2\mu - 1}{4} \Delta t \|l_{w,h}^n \nabla \varphi_{j,h}^{n+1}\|^2 + \frac{4\mu^2 \Delta t}{2\mu - 1} \|l_{w,h}^n \nabla \eta_{v,j}^{n+1}\|^2.
\end{aligned}$$

For the fourth and fifth nonlinear terms, we use Hölder's inequality, Sobolev embedding theorems, Poincaré and Young's inequalities to reveal

$$\begin{aligned}
\left| \left(\langle \psi_h \rangle^n \cdot \nabla (\mathbf{v}_j(t^{n+1}) - \mathbf{v}_j(t^n)), \varphi_{j,h}^{n+1} \right) \right| &\leq C \|\langle \psi_h \rangle^n\| \|\nabla (\mathbf{v}_j(t^{n+1}) - \mathbf{v}_j(t^n))\|_{L^6} \|\varphi_{j,h}^{n+1}\|_{L^3} \\
&\leq C \|\langle \psi_h \rangle^n\| \|\mathbf{v}_j(t^{n+1}) - \mathbf{v}_j(t^n)\|_{H^2} \|\varphi_{j,h}^{n+1}\|_{L^2}^{\frac{1}{2}} \|\nabla \varphi_{j,h}^{n+1}\|_{L^2}^{\frac{1}{2}} \\
&\leq C \|\langle \psi_h \rangle^n\| \|\mathbf{v}_j(t^{n+1}) - \mathbf{v}_j(t^n)\|_{H^2} \|\nabla \varphi_{j,h}^{n+1}\| \\
&\leq \frac{\alpha_j}{44} \|\nabla \varphi_{j,h}^{n+1}\|^2 + \frac{C}{\alpha_j} \Delta t^2 \|\langle \psi_h \rangle^n\|^2 \|\mathbf{v}_{j,t}(t^*)\|_{H^2}^2, \\
\left| \left(\psi_{j,h}^n \cdot \nabla \mathbf{v}_j(t^n), \varphi_{j,h}^{n+1} \right) \right| &\leq \frac{\alpha_j}{44} \|\nabla \varphi_{j,h}^{n+1}\|^2 + \frac{C}{\alpha_j} \|\psi_{j,h}^n\|^2 \|\mathbf{v}_j(t^n)\|_{H^2}^2.
\end{aligned}$$

For the sixth, seventh, eighth, and ninth nonlinear terms, apply Young's inequalities with (2.1) to obtain

$$\begin{aligned}
\left(\langle \eta_w \rangle^n \cdot \nabla (\mathbf{v}_j(t^{n+1}) - \mathbf{v}_j(t^n)), \varphi_{j,h}^{n+1} \right) &\leq C \|\nabla \langle \eta_w \rangle^n\| \|\nabla (\mathbf{v}_j(t^{n+1}) - \mathbf{v}_j(t^n))\| \|\nabla \varphi_{j,h}^{n+1}\| \\
&\leq \frac{\alpha_j}{44} \|\nabla \varphi_{j,h}^{n+1}\|^2 + \frac{C}{\alpha_j} \Delta t^2 \|\nabla \langle \eta_w \rangle^n\|^2 \|\nabla \mathbf{v}_{j,t}(t^{**})\|^2, \\
\left| \left(\langle \mathbf{w}_h \rangle^n \cdot \nabla \eta_{\mathbf{v},j}^{n+1}, \varphi_{j,h}^{n+1} \right) \right| &\leq C \|\nabla \langle \mathbf{w}_h \rangle^n\| \|\nabla \eta_{\mathbf{v},j}^{n+1}\| \|\nabla \varphi_{j,h}^{n+1}\| \\
&\leq \frac{\alpha_j}{44} \|\nabla \varphi_{j,h}^{n+1}\|^2 + \frac{C}{\alpha_j} \|\nabla \langle \mathbf{w}_h \rangle^n\|^2 \|\nabla \eta_{\mathbf{v},j}^{n+1}\|^2, \\
\left| \left(\mathbf{w}_{j,h}'^n \cdot \nabla \eta_{\mathbf{v},j}^n, \varphi_{j,h}^{n+1} \right) \right| &\leq C \|\nabla \mathbf{w}_{j,h}'^n\| \|\nabla \eta_{\mathbf{v},j}^n\| \|\nabla \varphi_{j,h}^{n+1}\| \\
&\leq \frac{\alpha_j}{44} \|\nabla \varphi_{j,h}^{n+1}\|^2 + \frac{C}{\alpha_j} \|\nabla \mathbf{w}_{j,h}'^n\|^2 \|\nabla \eta_{\mathbf{v},j}^n\|^2, \\
\left| \left(\eta_{\mathbf{w},j}^n \cdot \nabla \mathbf{v}_j(t^n), \varphi_{j,h}^{n+1} \right) \right| &\leq C \|\nabla \eta_{\mathbf{w},j}^n\| \|\nabla \mathbf{v}_j(t^n)\| \|\nabla \varphi_{j,h}^{n+1}\| \\
&\leq \frac{\alpha_j}{44} \|\nabla \varphi_{j,h}^{n+1}\|^2 + \frac{C}{\alpha_j} \|\nabla \eta_{\mathbf{w},j}^n\|^2 \|\nabla \mathbf{v}_j(t^n)\|^2.
\end{aligned}$$

Using Taylor's series, Cauchy-Schwarz and Young's inequalities, the last term is evaluated as

$$\begin{aligned}
\left| G_1(t, \mathbf{v}_j, \mathbf{w}_j, \varphi_{j,h}^{n+1}) \right| &\leq \frac{\alpha_j}{44} \|\nabla \varphi_{j,h}^{n+1}\|^2 + C \Delta t^2 \left(\|\mathbf{v}_{j,tt}(t_1^*)\|^2 + \|\nabla \mathbf{v}_{j,t}(t_2^*)\|^2 + \|\nabla \mathbf{w}_{j,t}(t_3^*)\|^2 \|\nabla \mathbf{v}_j(t^{n+1})\|^2 \right. \\
&\quad \left. + \|\nabla \mathbf{w}_{j,t}(t_4^*)\|^2 + \|\nabla (\mathbf{w}_j(t^n) - \langle \mathbf{w}(t^n) \rangle)\|^2 \|\nabla \mathbf{v}_{j,t}(t_5^*)\|^2 \right),
\end{aligned}$$

with $t_1^*, t_2^*, t_3^*, t_4^*, t_5^* \in [t^n, t^{n+1}]$. Using these estimates in (3.19) and reducing produces

$$\begin{aligned}
&\frac{1}{2\Delta t} \left(\|\varphi_{j,h}^{n+1}\|^2 - \|\varphi_{j,h}^n\|^2 \right) + \frac{1}{4\Delta t} \|\varphi_{j,h}^{n+1} - \varphi_{j,h}^n\|^2 + \frac{\bar{\nu} + \bar{\nu}_m}{4} \|\nabla \varphi_{j,h}^{n+1}\|^2 \\
&+ \frac{2\mu - 1}{4} \Delta t \|l_{w,h}^n \nabla \varphi_{j,h}^{n+1}\|^2 \leq \frac{|\nu_j - \nu_{m,j}|}{4} \|\nabla \psi_{j,h}^n\|^2 + \frac{|\nu_j' + \nu_{m,j}'|}{4} \|\nabla \varphi_{j,h}^n\|^2 \\
&+ \frac{11(\nu_j - \nu_{m,j})^2}{4\alpha_j} \|\nabla \eta_{\mathbf{w},j}^n\|^2 + \frac{11(\bar{\nu} + \bar{\nu}_m)^2}{4\alpha_j} \|\nabla \eta_{\mathbf{v},j}^{n+1}\|^2 + \frac{11(\nu_j' + \nu_{m,j}')^2}{4\alpha_j} \|\nabla \eta_{\mathbf{v},j}^n\|^2 \\
&+ C \frac{\mu^2 \Delta t^2}{\alpha_j} \|l_{w,h}^n\|_{L^4}^4 + \frac{4\mu^2 \Delta t}{2\mu - 1} \|l_{w,h}^n \nabla \eta_{\mathbf{v},j}^{n+1}\|^2 + \frac{C}{\alpha_j} \Delta t^2 \|\langle \psi_h \rangle^n\|^2 \|\mathbf{v}_{j,t}(t^*)\|_{H^2}^2 \\
&+ \frac{C}{\alpha_j} \|\psi_{j,h}^n\|^2 \|\mathbf{v}_j(t^n)\|_{H^2}^2 + \frac{C}{\alpha_j} \Delta t^2 \|\nabla \langle \eta_w \rangle^n\|^2 \|\nabla \mathbf{v}_{j,t}(t^{**})\|^2 + \frac{C}{\alpha_j} \|\nabla \langle \mathbf{w}_h \rangle^n\|^2 \|\nabla \eta_{\mathbf{v},j}^{n+1}\|^2 \\
&+ \frac{C}{\alpha_j} \|\nabla \mathbf{w}_{j,h}'^n\|^2 \|\nabla \eta_{\mathbf{v},j}^n\|^2 + \frac{C}{\alpha_j} \|\nabla \eta_{\mathbf{w},j}^n\|^2 \|\nabla \mathbf{v}_j(t^n)\|^2 + C \Delta t^2 \left(\|\mathbf{v}_{j,tt}(t_1^*)\|^2 + \|\nabla \mathbf{v}_{j,t}(t_2^*)\|^2 \right. \\
&\quad \left. + \|\nabla \mathbf{w}_{j,t}(t_3^*)\|^2 \|\nabla \mathbf{v}_j(t^{n+1})\|^2 + \|\nabla \mathbf{w}_{j,t}(t_4^*)\|^2 + \|\nabla (\mathbf{w}_j(t^n) - \langle \mathbf{w}(t^n) \rangle)\|^2 \|\nabla \mathbf{v}_{j,t}(t_5^*)\|^2 \right). \quad (3.21)
\end{aligned}$$

Applying similar techniques to (3.20), we get

$$\begin{aligned}
& \frac{1}{2\Delta t} \left(\|\psi_{j,h}^{n+1}\|^2 - \|\psi_{j,h}^n\|^2 \right) + \frac{1}{4\Delta t} \|\psi_{j,h}^{n+1} - \psi_{j,h}^n\|^2 + \frac{\bar{\nu} + \bar{\nu}_m}{4} \|\nabla \psi_{j,h}^{n+1}\|^2 \\
& + \frac{2\mu - 1}{4} \Delta t \|l_{v,h}^n \nabla \psi_{j,h}^{n+1}\|^2 \leq \frac{|\nu_j - \nu_{m,j}|}{4} \|\nabla \varphi_{j,h}^n\|^2 + \frac{|\nu'_j + \nu'_{m,j}|}{4} \|\nabla \psi_{j,h}^n\|^2 \\
& + \frac{11(\nu_j - \nu_{m,j})^2}{4\alpha_j} \|\nabla \eta_{v,j}^n\|^2 + \frac{11(\bar{\nu} + \bar{\nu}_m)^2}{4\alpha_j} \|\nabla \eta_{w,j}^{n+1}\|^2 + \frac{11(\nu'_j + \nu'_{m,j})^2}{4\alpha_j} \|\nabla \eta_{w,j}^n\|^2 \\
& + C \frac{\mu^2 \Delta t^2}{\alpha_j} \|l_{v,h}^n\|_{L^4}^4 + \frac{4\mu^2 \Delta t}{2\mu - 1} \|l_{v,h}^n \nabla \eta_{w,j}^{n+1}\|^2 + \frac{C}{\alpha_j} \Delta t^2 \|\langle \varphi_h \rangle^n\|^2 \|\mathbf{w}_{j,t}(s^*)\|_{\mathbf{H}^2}^2 \\
& + \frac{C}{\alpha_j} \|\varphi_{j,h}^n\|^2 \|\mathbf{w}_j(t^n)\|_{\mathbf{H}^2}^2 + \frac{C}{\alpha_j} \Delta t^2 \|\nabla \langle \eta_v \rangle^n\|^2 \|\nabla \mathbf{w}_{j,t}(s^{**})\|^2 + \frac{C}{\alpha_j} \|\nabla \langle \mathbf{v}_h \rangle^n\|^2 \|\nabla \eta_{w,j}^{n+1}\|^2 \\
& + \frac{C}{\alpha_j} \|\nabla \mathbf{v}'_{j,h}\|^2 \|\nabla \eta_{w,j}^n\|^2 + \frac{C}{\alpha_j} \|\nabla \eta_{v,j}^n\|^2 \|\nabla \mathbf{w}_j(t^n)\|^2 + C \Delta t^2 \left(\|\mathbf{w}_{j,t}(s_1^*)\|^2 + \|\nabla \mathbf{w}_{j,t}(s_2^*)\|^2 \right. \\
& \left. + \|\nabla \mathbf{v}_{j,t}(s_3^*)\|^2 \|\nabla \mathbf{w}_j(t^{n+1})\|^2 + \|\nabla \mathbf{v}_{j,t}(s_4^*)\|^2 + \|\nabla (\mathbf{v}_j(t^n) - \langle \mathbf{v}(t^n) \rangle)\|^2 \|\nabla \mathbf{w}_{j,t}(s_5^*)\|^2 \right), \quad (3.22)
\end{aligned}$$

with $s_1^*, s_2^*, s_3^*, s_4^*, s_5^* \in [t^n, t^{n+1}]$. Adding (3.21) and (3.22), assuming $\mu > 1/2$, dropping non-negative terms from left, multiplying both sides by $2\Delta t$, using regularity assumptions, $\|\varphi_{j,h}^0\| = \|\psi_{j,h}^0\| = \|\nabla \varphi_{j,h}^0\| = \|\nabla \psi_{j,h}^0\| = 0$, $\Delta t M = T$, and sum over the time-steps to find

$$\begin{aligned}
& \|\varphi_{j,h}^M\|^2 + \|\psi_{j,h}^M\|^2 + \frac{\bar{\nu} + \bar{\nu}_m}{2} \Delta t \left(\|\nabla \varphi_{j,h}^M\|^2 + \|\nabla \psi_{j,h}^M\|^2 \right) \\
& + \frac{\alpha_j \Delta t}{2} \sum_{n=1}^{M-1} \left(\|\nabla \varphi_{j,h}^n\|^2 + \|\nabla \psi_{j,h}^n\|^2 \right) \leq C \Delta t \frac{\mu^2 \Delta t^2}{\alpha_j} \sum_{n=0}^{M-1} \left(\|l_{v,h}^n\|_{L^4}^4 + \|l_{w,h}^n\|_{L^4}^4 \right) \\
& + \frac{8\mu^2 \Delta t^2}{2\mu - 1} \sum_{n=0}^{M-1} \left(\|l_{v,h}^n \nabla \eta_{w,j}^{n+1}\|^2 + \|l_{w,h}^n \nabla \eta_{v,j}^{n+1}\|^2 \right) \\
& + \frac{C}{\alpha_j} \Delta t^2 \sum_{n=1}^{M-1} \Delta t \left(\|\langle \varphi_h \rangle^n\|^2 \|\mathbf{w}_{j,t}(t)\|_{L^\infty(0,T;\mathbf{H}^2(\Omega))}^2 + \|\langle \psi_h \rangle^n\|^2 \|\mathbf{v}_{j,t}(t)\|_{L^\infty(0,T;\mathbf{H}^2(\Omega))}^2 \right) \\
& + \frac{C \Delta t}{\alpha_j} \sum_{n=1}^{M-1} \left(\|\varphi_{j,h}^n\|^2 \|\mathbf{w}_j(t)\|_{L^\infty(0,T;\mathbf{H}^2(\Omega))}^2 + \|\psi_{j,h}^n\|^2 \|\mathbf{v}_j(t)\|_{L^\infty(0,T;\mathbf{H}^2(\Omega))}^2 \right) \\
& + \frac{C}{\alpha_j} \sum_{n=0}^{M-1} \Delta t \left(\|\nabla \langle \mathbf{v}_h \rangle^n\|^2 \|\nabla \eta_{w,j}^{n+1}\|^2 + \|\nabla \langle \mathbf{w}_h \rangle^n\|^2 \|\nabla \eta_{v,j}^{n+1}\|^2 \right) \\
& + \frac{C}{\alpha_j} \sum_{n=0}^{M-1} \Delta t \left(\|\nabla \mathbf{v}'_{j,h}\|^2 \|\nabla \eta_{w,j}^n\|^2 + \|\nabla \mathbf{w}'_{j,h}\|^2 \|\nabla \eta_{v,j}^n\|^2 \right) + CT \left(\Delta t^2 + \frac{h^{2k}}{\alpha_j} + \frac{h^{2k} \Delta t^2}{\alpha_j} \right). \quad (3.23)
\end{aligned}$$

For the first sum on the right-hand-side, we get different bounds for 2D and 3D due to different Sobolev embedding:

$$\begin{aligned}
2D : \quad & \|l_{v,h}^n\|_{L^4}^4 \leq C \max_j \|\mathbf{v}'_{j,h}\|^2 \|\nabla \mathbf{v}'_{j,h}\|^2 \leq C \max_j \|\nabla \mathbf{v}'_{j,h}\|^2, \\
3D : \quad & \|l_{v,h}^n\|_{L^4}^4 \leq C \max_j \|\mathbf{v}'_{j,h}\| \|\nabla \mathbf{v}'_{j,h}\|^3 \leq C \max_j \|\nabla \mathbf{v}'_{j,h}\|^3,
\end{aligned}$$

where the second upper bound in each inequality coming from the stability theorem, and similarly for $\mathbf{w}'_{j,h}$. With the inverse inequality and the stability bound (used on the L^2 norm), we obtain

$$\|\nabla \mathbf{v}'_{j,h}\| \leq Ch^{-1} \|\mathbf{v}'_{j,h}\| \leq Ch^{-1}.$$

Thus, the bounds for both 2D or 3D:

$$\begin{aligned}\|l_{v,h}^n\|_{L^4}^4 &\leq Ch^{2-d} \max_j \|\nabla \mathbf{v}_{j,h}'^n\|^2, \\ \|l_{w,h}^n\|_{L^4}^4 &\leq Ch^{2-d} \max_j \|\nabla \mathbf{w}_{j,h}'^n\|^2.\end{aligned}$$

Using these bounds and the stability bound, the first sum on the right is bounded as

$$\begin{aligned}C\Delta t \frac{\mu^2 \Delta t^2}{\alpha_j} \sum_{n=0}^{M-1} (\|l_{v,h}^n\|_{L^4}^4 + \|l_{w,h}^n\|_{L^4}^4) &\leq Ch^{2-d} \Delta t \frac{\mu^2 \Delta t^2}{\alpha_j} \max_j (\|\nabla \mathbf{v}_{j,h}'^n\|^2 + \|\nabla \mathbf{w}_{j,h}'^n\|^2) \\ &\leq Ch^{2-d} \frac{\mu^2 \Delta t^2}{\alpha_j}.\end{aligned}$$

For the first part (the second part follows analogously) of the second sum on the right in (3.23), we use Agmon's inequality [41], the inverse inequality [5], standard estimates of the L^2 projection error in the H^1 norm for the finite element functions, and the stability estimate to obtain

$$\begin{aligned}\Delta t^2 \sum_{n=0}^{M-1} \|l_{v,h}^n \nabla \boldsymbol{\eta}_{\mathbf{w},j}^{n+1}\|^2 &\leq \Delta t^2 \sum_{n=0}^{M-1} \|l_{v,h}^n\|_{\infty}^2 \|\nabla \boldsymbol{\eta}_{\mathbf{w},j}^{n+1}\|^2 \\ &\leq Ch^{-1} \Delta t^2 \sum_{n=0}^{M-1} \left(\max_j \|\nabla \mathbf{v}_{j,h}'^n\|^2 \right) \|\nabla \boldsymbol{\eta}_{\mathbf{w},j}^{n+1}\|^2 \\ &\leq Ch^{2k-1} \Delta t^2 \sum_{n=0}^{M-1} \left(\max_j \|\nabla \mathbf{v}_{j,h}'^n\|^2 \right) |\mathbf{w}_j^{n+1}|_{k+1}^2 \\ &\leq Ch^{2k-1} \Delta t.\end{aligned}$$

Using the above bounds, stability estimate, and standard bounds for $\|\nabla \boldsymbol{\eta}_{\mathbf{v},j}\|$ and $\|\nabla \boldsymbol{\eta}_{\mathbf{w},j}\|$, we have

$$\begin{aligned}\|\boldsymbol{\varphi}_{j,h}^M\|^2 + \|\boldsymbol{\psi}_{j,h}^M\|^2 + \frac{\bar{\nu} + \bar{\nu}_m}{2} \Delta t \left(\|\nabla \boldsymbol{\varphi}_{j,h}^M\|^2 + \|\nabla \boldsymbol{\psi}_{j,h}^M\|^2 \right) &+ \frac{\alpha_j \Delta t}{2} \sum_{n=1}^{M-1} \left(\|\nabla \boldsymbol{\varphi}_{j,h}^n\|^2 + \|\nabla \boldsymbol{\psi}_{j,h}^n\|^2 \right) \\ &\leq \frac{C}{\alpha_j} \Delta t^2 \sum_{n=1}^{M-1} \Delta t \left(\|\langle \boldsymbol{\varphi}_h \rangle^n\|^2 \|\mathbf{w}_{j,t}(t)\|_{L^\infty(0,T;\mathbf{H}^2(\Omega))}^2 + \|\langle \boldsymbol{\psi}_h \rangle^n\|^2 \|\mathbf{v}_{j,t}(t)\|_{L^\infty(0,T;\mathbf{H}^2(\Omega))}^2 \right) \\ &+ \frac{C \Delta t}{\alpha_j} \sum_{n=1}^{M-1} \left(\|\boldsymbol{\varphi}_{j,h}^n\|^2 \|\mathbf{w}_j(t)\|_{L^\infty(0,T;\mathbf{H}^2(\Omega))}^2 + \|\boldsymbol{\psi}_{j,h}^n\|^2 \|\mathbf{v}_j(t)\|_{L^\infty(0,T;\mathbf{H}^2(\Omega))}^2 \right) \\ &+ C(\Delta t^2 + h^{2k} + h^{2k} \Delta t^2 + h^{2-d} \Delta t^2 + h^{2k-1} \Delta t).\end{aligned}\tag{3.24}$$

Sum over $j = 1, \dots, J$, and apply triangle and Young's inequalities, to get

$$\begin{aligned}\sum_{j=1}^J \|\boldsymbol{\varphi}_{j,h}^M\|^2 + \sum_{j=1}^J \|\boldsymbol{\psi}_{j,h}^M\|^2 &+ \frac{\alpha_j \Delta t}{2} \sum_{n=1}^M \sum_{j=1}^J \left(\|\nabla \boldsymbol{\varphi}_{j,h}^n\|^2 + \|\nabla \boldsymbol{\psi}_{j,h}^n\|^2 \right) \\ &\leq \frac{C}{\alpha_j} \sum_{n=1}^{M-1} \left(\frac{\Delta t^3}{J} + \Delta t \right) \left(\sum_{j=1}^J \|\boldsymbol{\varphi}_{j,h}^n\|^2 + \sum_{j=1}^J \|\boldsymbol{\psi}_{j,h}^n\|^2 \right) \\ &+ CJ(\Delta t^2 + h^{2k} + h^{2k} \Delta t^2 + h^{2-d} \Delta t^2 + h^{2k-1} \Delta t).\end{aligned}\tag{3.25}$$

Applying the discrete Grönwall Lemma 2.1, we have

$$\begin{aligned}\sum_{j=1}^J \|\boldsymbol{\varphi}_{j,h}^M\|^2 + \sum_{j=1}^J \|\boldsymbol{\psi}_{j,h}^M\|^2 &+ \frac{\alpha_j \Delta t}{2} \sum_{n=1}^M \sum_{j=1}^J \left(\|\nabla \boldsymbol{\varphi}_{j,h}^n\|^2 + \|\nabla \boldsymbol{\psi}_{j,h}^n\|^2 \right) \\ &\leq \exp \left(\frac{CT}{\alpha_j} \left(1 + \frac{\Delta t^2}{J} \right) \right) (\Delta t^2 + h^{2k} + h^{2k} \Delta t^2 + h^{2-d} \Delta t^2 + h^{2k-1} \Delta t).\end{aligned}\tag{3.26}$$

Now using the triangle and inequality we can write

$$\begin{aligned}
& \sum_{j=1}^J \|e_{v,j}^M\|^2 + \sum_{j=1}^J \|e_{w,j}^M\|^2 + \frac{\alpha_j \Delta t}{2} \sum_{n=1}^M \sum_{j=1}^J \left(\|\nabla e_{v,j}^n\|^2 + \|\nabla e_{w,j}^n\|^2 \right) \\
& \leq 2 \left(\sum_{j=1}^J \|\varphi_{j,h}^M\|^2 + \sum_{j=1}^J \|\eta_{v,j}^M\|^2 + \sum_{j=1}^J \|\psi_{j,h}^M\|^2 + \sum_{j=1}^J \|\eta_{w,j}^M\|^2 \right) \\
& \quad + \frac{\alpha_j \Delta t}{2} \sum_{n=1}^M \sum_{j=1}^J \left(\|\nabla \varphi_{j,h}^n\|^2 + \|\nabla \eta_{v,j}^n\|^2 + \|\nabla \psi_{j,h}^n\|^2 + \|\nabla \eta_{w,j}^n\|^2 \right) \\
& \leq C \exp \left(\frac{CT}{\alpha_j} \left(1 + \frac{\Delta t^2}{J} \right) \right) (\Delta t^2 + h^{2k} + h^{2k} \Delta t^2 + h^{2-d} \Delta t^2 + h^{2k-1} \Delta t + h^{2k+2}). \quad (3.27)
\end{aligned}$$

Finally, again the use of triangle and Young's inequality completes the proof. \square

4. Numerical experiments. As the proposed algorithm is decoupled, at each time-step, we have two Oseen-type problems for each of the J realizations. For MHD simulation, the pointwise enforcement of the solenoidal constraint is crucial [16]. In this paper, for all numerical experiments, we use stable (P_2, P_1^{disc}) Scott-Vogelius elements on barycenter refined regular triangular meshes for each of the Oseen-type problem [2]. The Scott-Vogelius element is pointwise divergence-free and thus allows to enforce the continuity equations $\nabla \cdot \mathbf{u}_j = 0$ and the solenoidal constraints $\nabla \cdot \mathbf{B}_j = 0$ in the discrete level, up to round-off error. Thus, we approximate the Elsässer variables \mathbf{v}_j , and \mathbf{w}_j with a quadratic finite element and q_j , and r_j with a linear finite element solving problem with the proposed scheme (3.1)-(3.2). We consider the tuning parameter $\mu = 1$, number of realizations $J = 20$, and the index $j = 1, 2, \dots, J$ in all experiments. We write the codes, draw the geometries, and generate the regular triangular meshes in Freefem++[13]. In the first experiment, we test the predicted convergence rates, while the second experiment shows the energy stability of the scheme, and in the third and fourth experiments, we show that the scheme performs well in benchmark lid-driven cavity, and channel flow past a step, respectively.

4.1. Convergence rate verification. To verify the spatial and temporal convergence rates, we consider a domain $\Omega = (0, 1)^2$ and create structured meshes for $h = 1/4, 1/8, 1/16, 1/32$, and $1/64$ using successive refinements. We consider two independent and uniformly distributed random samples for the kinematic viscosity and magnetic diffusivity pair $\{(\nu_j, \nu_{m,j}) \in [0.009, 0.011] \times [0.09, 0.11]\}$, and $\{(\nu_j, \nu_{m,j}) \in [0.009, 0.011] \times [0.0009, 0.0011]\}$ with mean $(\bar{\nu}, \bar{\nu}_m) = (0.01, 0.1)$, and $(0.01, 0.001)$, respectively. For both samples we consider, the conditions $\alpha_j > 0$ hold true. Instead of computing the solution for each pair independently and then taking their average, we compute the average of these J independent solutions by using the proposed ensemble Algorithm 1.

For this experiment, we begin with the following analytical functions

$$\mathbf{v} = \begin{pmatrix} \cos y + (1 + e^t) \sin y \\ \sin x + (1 + e^t) \cos x \end{pmatrix}, \quad \mathbf{w} = \begin{pmatrix} \cos y - (1 + e^t) \sin y \\ \sin x - (1 + e^t) \cos x \end{pmatrix}, \quad p = \sin(x + y)(1 + e^t), \quad \text{and } \lambda = 0. \quad (4.1)$$

Next, we consider J different manufactured solutions introducing a perturbation parameter ϵ as

$$\mathbf{v}_j(x, y, t) := \left(1 + \frac{(-1)^{j+1} \lceil j/2 \rceil}{5} \epsilon \right) \mathbf{v}, \quad \text{and } \mathbf{w}_j(x, y, t) := \left(1 + \frac{(-1)^{j+1} \lceil j/2 \rceil}{5} \epsilon \right) \mathbf{w}. \quad (4.2)$$

The above exact solutions are divergence-free. For each pair $(\nu_j, \nu_{m,j})$, using the above exact solutions, we compute the forcing vectors from (1.7)-(1.8). We use $\mathbf{v}_j^0 = \mathbf{v}_j(x, y, 0)$, and $\mathbf{w}_j^0 = \mathbf{w}_j(x, y, 0)$ as the initial conditions and $\mathbf{v}_j|_{\partial\Omega} = \mathbf{v}_j$, and $\mathbf{w}_j|_{\partial\Omega} = \mathbf{w}_j$ as the boundary conditions.

The ensemble average error is defined as $\langle \mathbf{e}_z \rangle^n := \langle \mathbf{z}_h \rangle^n - \langle \mathbf{z}(t^n) \rangle$, where $\mathbf{z} = \mathbf{v}$ or \mathbf{w} , which reduces to $\langle \mathbf{e}_z \rangle^n = \langle \mathbf{z}_h \rangle^n - \mathbf{z}(t^n)$. We compute the $L^2(0, T; \mathbf{H}^1)$ norm of the error and is denoted by $\|\cdot\|_{2,1}$.

For the spatial convergence, we consider a small end time $T = 0.001$ so that the temporal error does not dominate over the spatial error, and use a fixed time-step size $\Delta t = T/8$. We run a complete simulation beginning with $h = 1/4$ and repeat with the successively refined meshes until we have $h = 1/64$. In Tables 4.1-4.3, we list the norm of the spatial errors and compute the spatial convergence

Spatial convergence (fixed $T = 0.001$, $\Delta t = T/8$) with $j = 1, 2, \dots, 20$								
$\epsilon = 0.0$	$\{(\nu_j, \nu_{m,j}) \in [0.009, 0.011] \times [0.09, 0.11]\}$				$\{(\nu_j, \nu_{m,j}) \in [0.009, 0.011] \times [0.0009, 0.0011]\}$			
h	$\ \langle \mathbf{e}_v \rangle\ _{2,1}$	rate	$\ \langle \mathbf{e}_w \rangle\ _{2,1}$	rate	$\ \langle \mathbf{e}_v \rangle\ _{2,1}$	rate	$\ \langle \mathbf{e}_w \rangle\ _{2,1}$	rate
$\frac{1}{4}$	1.0741e-04		2.0597e-04		1.0752e-04		2.0602e-04	
$\frac{1}{8}$	2.7081e-05	1.99	5.1620e-05	2.00	2.7108e-05	1.99	5.1653e-05	2.00
$\frac{1}{16}$	6.8025e-06	1.99	1.2957e-05	1.99	6.8037e-06	1.99	1.3009e-05	1.99
$\frac{1}{32}$	1.7168e-06	1.99	3.2523e-06	1.99	1.7110e-06	1.99	3.3181e-06	1.97
$\frac{1}{64}$	4.3049e-07	2.00	8.1168e-07	2.00	4.3117e-07	1.99	8.5456e-07	1.96

Table 4.1: Spatial errors and convergence rates for \mathbf{v} and \mathbf{w} with $\epsilon = 0.0$.

Spatial convergence (fixed $T = 0.001$, $\Delta t = T/8$) with $j = 1, 2, \dots, 20$								
$\epsilon = 0.001$	$\{(\nu_j, \nu_{m,j}) \in [0.009, 0.011] \times [0.09, 0.11]\}$				$\{(\nu_j, \nu_{m,j}) \in [0.009, 0.011] \times [0.0009, 0.0011]\}$			
h	$\ \langle \mathbf{e}_v \rangle\ _{2,1}$	rate	$\ \langle \mathbf{e}_w \rangle\ _{2,1}$	rate	$\ \langle \mathbf{e}_v \rangle\ _{2,1}$	rate	$\ \langle \mathbf{e}_w \rangle\ _{2,1}$	rate
$\frac{1}{4}$	1.0741e-04		2.0597e-04		1.0752e-04		2.0602e-04	
$\frac{1}{8}$	2.7081e-05	1.99	5.1620e-05	2.00	2.7108e-05	1.99	5.1653e-05	2.00
$\frac{1}{16}$	6.8025e-06	1.99	1.2957e-05	1.99	6.8037e-06	1.99	1.3009e-05	1.99
$\frac{1}{32}$	1.7168e-06	1.99	3.2523e-06	1.99	1.7110e-06	1.99	3.3181e-06	1.97
$\frac{1}{64}$	4.3048e-07	2.00	8.1168e-07	2.00	4.3123e-07	1.99	8.5458e-07	1.96

Table 4.2: Spatial errors and convergence rates for \mathbf{v} and \mathbf{w} with $\epsilon = 0.001$.

Spatial convergence (fixed $T = 0.001$, $\Delta t = T/8$) with $j = 1, 2, \dots, 20$								
$\epsilon = 0.01$	$\{(\nu_j, \nu_{m,j}) \in [0.009, 0.011] \times [0.09, 0.11]\}$				$\{(\nu_j, \nu_{m,j}) \in [0.009, 0.011] \times [0.0009, 0.0011]\}$			
h	$\ \langle \mathbf{e}_v \rangle\ _{2,1}$	rate	$\ \langle \mathbf{e}_w \rangle\ _{2,1}$	rate	$\ \langle \mathbf{e}_v \rangle\ _{2,1}$	rate	$\ \langle \mathbf{e}_w \rangle\ _{2,1}$	rate
$\frac{1}{4}$	1.0741e-04		2.0597e-04		1.0752e-04		2.0602e-04	
$\frac{1}{8}$	2.7081e-05	1.99	5.1620e-05	2.00	2.7108e-05	1.99	5.1653e-05	2.00
$\frac{1}{16}$	6.8031e-06	1.99	1.2957e-05	1.99	6.8046e-06	1.99	1.3009e-05	1.99
$\frac{1}{32}$	1.7182e-06	1.99	3.2527e-06	1.99	1.7146e-06	1.99	3.3186e-06	1.97
$\frac{1}{64}$	4.3552e-07	1.98	8.1418e-07	2.00	4.5043e-07	1.93	8.6250e-07	1.94

Table 4.3: Spatial errors and convergence rates for \mathbf{v} and \mathbf{w} with $\epsilon = 0.01$.

Temporal convergence (fixed $h = 1/64$, $T = 1$) with $j = 1, 2, \dots, 20$								
$\epsilon = 0.0$	$\{(\nu_j, \nu_{m,j}) \in [0.009, 0.011] \times [0.09, 0.11]\}$				$\{(\nu_j, \nu_{m,j}) \in [0.009, 0.011] \times [0.0009, 0.0011]\}$			
Δt	$\ \langle \mathbf{e}_v \rangle\ _{2,1}$	rate	$\ \langle \mathbf{e}_w \rangle\ _{2,1}$	rate	$\ \langle \mathbf{e}_v \rangle\ _{2,1}$	rate	$\ \langle \mathbf{e}_w \rangle\ _{2,1}$	rate
$\frac{T}{2}$	2.2419e-01		1.6653e-01		9.5227e-01		7.5549e-01	
$\frac{T}{4}$	1.0851e-01	1.05	7.9697e-02	1.06	5.2621e-01	0.86	4.5248e-01	0.74
$\frac{T}{8}$	5.5987e-02	0.95	4.0986e-02	0.96	3.0570e-01	0.78	2.7650e-01	0.71
$\frac{T}{16}$	2.9231e-02	0.94	2.1480e-02	0.93	1.7541e-01	0.80	1.6320e-01	0.76
$\frac{T}{32}$	1.5075e-02	0.96	1.1117e-02	0.95	9.6367e-02	0.86	9.0908e-02	0.84
$\frac{T}{64}$	7.6728e-03	0.97	5.6704e-03	0.97	5.0830e-02	0.92	4.8256e-02	0.91
$\frac{T}{128}$	3.8730e-03	0.99	2.8659e-03	0.98	2.6137e-02	0.96	2.4887e-02	0.96

Table 4.4: Temporal errors and convergence rates for \mathbf{v} and \mathbf{w} with $\epsilon = 0.0$.

rates for the two sets of samples of the viscosity pair, for several choices of ϵ . In each case, we observe a second order spatial convergence, which is predicted by our error analysis given in Theorem 3.2.

To observe the temporal convergence rates, we use a fixed $h = 1/64$, and the simulation end time $T = 1$ and run the simulations varying the time-step size as $\Delta t = T/2, T/4, T/8, T/16, T/32, T/64$, and $T/128$. In Tables 4.4-4.6, we represent the $L^2(0, T; \mathbf{H}^1)$ norm of the temporal errors and their convergence rates. As $\Delta t \rightarrow 0$, we observe a first order temporal convergence rate, which is also consistent with the theoretical analysis in Theorem 3.2.

Temporal convergence (fixed $h = 1/64$, $T = 1$) with $j = 1, 2, \dots, 20$								
$\epsilon = 0.001$	$\{(\nu_j, \nu_{m,j}) \in [0.009, 0.011] \times [0.09, 0.11]\}$				$\{(\nu_j, \nu_{m,j}) \in [0.009, 0.011] \times [0.0009, 0.0011]\}$			
Δt	$\ \langle \mathbf{e}_v \rangle\ _{2,1}$	rate	$\ \langle \mathbf{e}_w \rangle\ _{2,1}$	rate	$\ \langle \mathbf{e}_v \rangle\ _{2,1}$	rate	$\ \langle \mathbf{e}_w \rangle\ _{2,1}$	rate
$\frac{T}{2}$	2.2417e-01		1.6646e-01		9.5155e-01		7.5403e-01	
$\frac{T}{4}$	1.0850e-01	1.05	7.9669e-02	1.06	5.2583e-01	0.86	4.5182e-01	0.74
$\frac{T}{8}$	5.5981e-02	0.95	4.0972e-02	0.96	3.0551e-01	0.78	2.7619e-01	0.71
$\frac{T}{16}$	2.9228e-02	0.94	2.1473e-02	0.93	1.7532e-01	0.80	1.6307e-01	0.76
$\frac{T}{32}$	1.5073e-02	0.96	1.1114e-02	0.95	9.6320e-02	0.86	9.0848e-02	0.84
$\frac{T}{64}$	7.6711e-03	0.97	5.6682e-03	0.97	5.0802e-02	0.92	4.8223e-02	0.91
$\frac{T}{128}$	3.8715e-03	0.99	2.8645e-03	0.98	2.6115e-02	0.96	2.4862e-02	0.96

Table 4.5: Temporal errors and convergence rates for \mathbf{v} and \mathbf{w} with $\epsilon = 0.001$.

Temporal convergence (fixed $h = 1/64$, $T = 1$) with $j = 1, 2, \dots, 20$								
$\epsilon = 0.01$	$\{(\nu_j, \nu_{m,j}) \in [0.009, 0.011] \times [0.09, 0.11]\}$				$\{(\nu_j, \nu_{m,j}) \in [0.009, 0.011] \times [0.0009, 0.0011]\}$			
Δt	$\ \langle \mathbf{e}_v \rangle\ _{2,1}$	rate	$\ \langle \mathbf{e}_w \rangle\ _{2,1}$	rate	$\ \langle \mathbf{e}_v \rangle\ _{2,1}$	rate	$\ \langle \mathbf{e}_w \rangle\ _{2,1}$	rate
$\frac{T}{2}$	2.2247e-01		1.6093e-01		8.9271e-01		6.4701e-01	
$\frac{T}{4}$	1.0787e-01	1.04	7.7193e-02	1.06	4.9474e-01	0.85	3.9981e-01	0.69
$\frac{T}{8}$	5.5785e-02	0.95	3.9847e-02	0.95	2.8963e-01	0.77	2.5194e-01	0.67
$\frac{T}{16}$	2.9250e-02	0.93	2.1008e-02	0.92	1.6848e-01	0.78	1.5314e-01	0.72
$\frac{T}{32}$	1.5207e-02	0.94	1.0976e-02	0.94	9.4351e-02	0.84	8.7772e-02	0.80
$\frac{T}{64}$	7.8585e-03	0.95	5.6893e-03	0.95	5.0981e-02	0.89	4.7969e-02	0.87
$\frac{T}{128}$	4.0843e-03	0.94	2.9624e-03	0.94	2.7116e-02	0.91	2.5650e-02	0.90

Table 4.6: Temporal errors and convergence rates for \mathbf{v} and \mathbf{w} with $\epsilon = 0.01$.

4.2. Energy stability test. To test the energy stability of the proposed scheme (3.1)-(3.2), we keep the same domain, the initial conditions with $\epsilon = 0.01$, and the finite element pairs as given in the previous experiment 4.1. A uniformly distributed random of sample $\{(\nu_j, \nu_{m,j}) \in [0.009, 0.011] \times [0.09, 0.11]\}$ with mean $(\bar{\nu}, \bar{\nu}_m) = (0.01, 0.1)$ is considered, so that $\alpha_j > 0$, for all j . Clearly, the sample has a maximum 10% fluctuation from the mean. We consider homogeneous boundary conditions for the velocity and magnetic field, and zero body forces (i.e. $\mathbf{f}_j = \mathbf{g}_j = \mathbf{0}$) so that the system does not have any external source of energy. We choose $h = 1/32$, time-step size $\Delta t = 0.05$, and solve the problem in (1.7)-(1.8) by the proposed Algorithm 1. We define the energy of the system as:

$$E_h^n := \frac{1}{2} (\|\langle \mathbf{v}_h \rangle^n\|^2 + \|\langle \mathbf{w}_h \rangle^n\|^2).$$

The time evolution of energy until the end time $T = 1$ is showing in Fig. 4.1. We observe that the system is energy dissipation, and is consistent with the stability result in Theorem 3.1.

4.3. Lid-driven cavity. In this test, we consider a 2D benchmark regularized lid-driven cavity problem [3, 7, 28] with domain $\Omega = (-1, 1)^2$. No-slip boundary condition for the velocity is enforced on all boundaries except the top (which is the lid of the cavity), where we impose

$$\mathbf{u}_j = \left(1 + \frac{(-1)^{j+1} \lceil j/2 \rceil}{5} \epsilon\right) \begin{pmatrix} (1 - x^2)^2 \\ 0 \end{pmatrix}.$$

For the magnetic field boundary conditions, we assign

$$\mathbf{B}_j = \left(1 + \frac{(-1)^{j+1} \lceil j/2 \rceil}{5} \epsilon\right) \begin{pmatrix} 0 \\ 1 \end{pmatrix}$$

on all sides. We assume the flow begins from rest, initially there is no magnetic field, and no external source is present in the system (i.e. $\mathbf{f}_j = \mathbf{g}_j = \mathbf{0}$). We generate a computational mesh that provides a total of 1,307,690 degrees of freedom (dofs) for each of velocity and magnetic field and a total of 163,702 dofs for each of pressure and magnetic pressure.

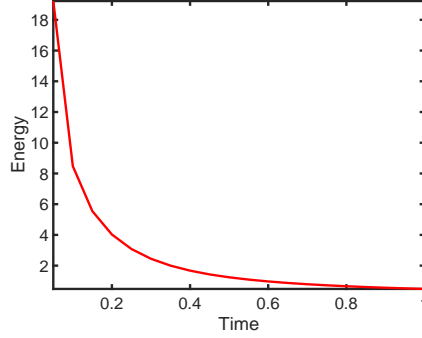
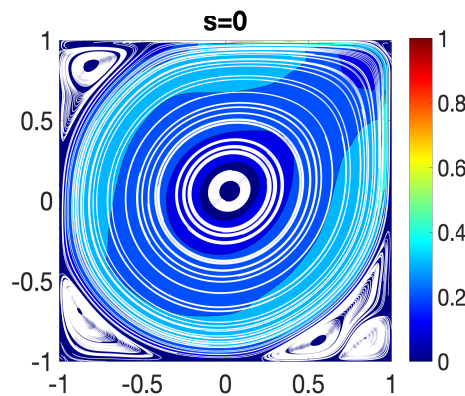


Fig. 4.1: Energy of the MHD system versus time.

To study the long-time unsteady flow behavior, we first validate our computation with available data from the literature [7]. Thus, we run a simulation in absence of the magnetic field (setting $s = 0$ in the model) with the Reynolds number $Re = 15000$ (that is, no perturbation in the viscosities, initial and boundary conditions are considered). We define the viscosity $\nu = 2/Re$, since the maximum velocity of the lid is 1 and the characteristic length is 2. Thanks to the unconditional stability, we run the simulation with a large time-step size $\Delta t = 5$ until the end $T = 600$ and plot the solution in Fig. 4.2. We observe a large primary vortex in the center of the cavity, and other vortices are near to the three corners except for the upper right. We note that the same observation was made by Fick et al. in [7].

Next, we consider a total of 20 uniformly distributed random Reynolds numbers and magnetic diffusivities from the intervals $[13636.36, 16666.67]$ and $[0.009, 0.011]$, respectively. That is, the sample mean of the Reynolds numbers and the sample mean of the magnetic diffusivities are 15151.52, and 0.01, respectively.

We run the simulations for several values of the coupling parameter s with a fixed $\epsilon = 0.01$ and plot the velocity (speed contour) and magnetic field (strength) solutions at $T = 600$ in Figures 4.3-4.4. From the speed contour plots, Fig. 4.3, as s increases, a change in the flow structure is observed and with $s = 1$, the center of the circulation gets close to $(0, 0)$ and the magnetic field strength realizes a type of reflection symmetry.

Fig. 4.2: A lid-driven cavity problem. Velocity solution (shown as streamlines over speed contours) for $Re = 15000$.

4.4. MHD channel flow over a step. In this experiment, we consider a benchmark problem [1, 14, 27, 35] in which the domain under consideration is a 30×10 rectangular channel with a 1×1

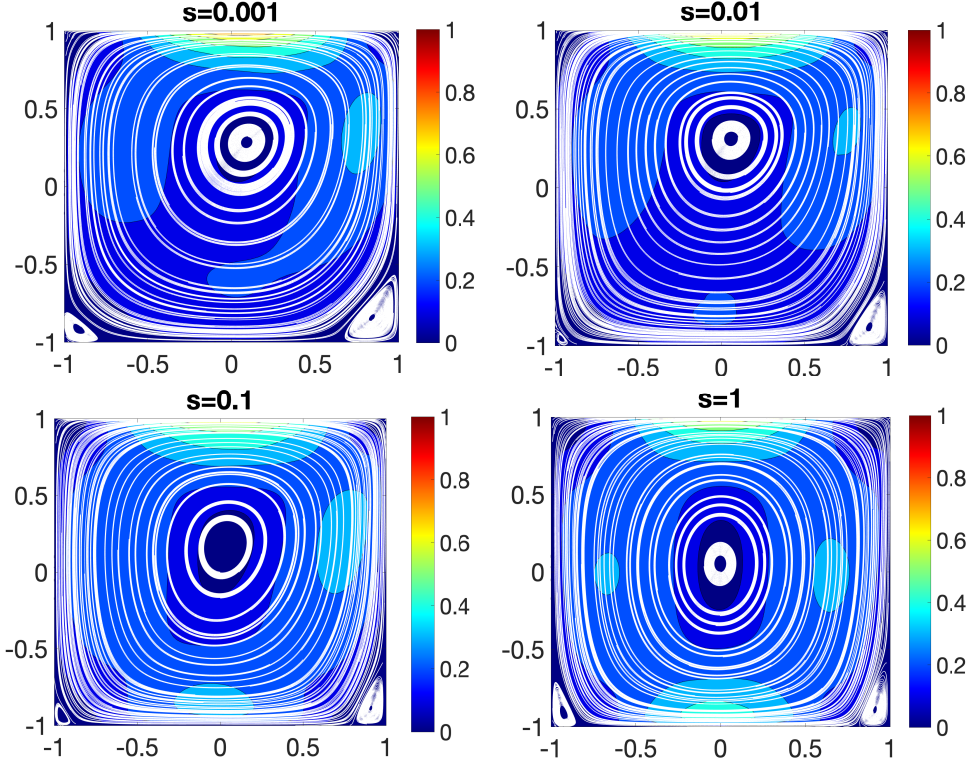


Fig. 4.3: A lid-driven cavity problem. The velocity ensemble average solutions for $13636.36 \leq Re_j \leq 16666.67$ at $T = 600$ for various coupling parameter s .

step at the bottom and five units away from the inlet. The problem is not physically accurate as the domain is not convex, but we run the simulation anyway. The following initial conditions are chosen:

$$\mathbf{u}_j^0 = \left(1 + \frac{(-1)^{j+1} \lceil j/2 \rceil}{5} \epsilon\right) \begin{pmatrix} \frac{y(10-y)}{25} \\ 0 \end{pmatrix}, \text{ and } \mathbf{B}_j^0 = \begin{pmatrix} 0 \\ 0 \end{pmatrix}.$$

The unperturbed ($\epsilon = 0$) initial velocity has a parabolic profile along the downstream direction and attains its maximum $\|\mathbf{u}_{max}^0\| = 1$ at $y = 5$, on the other hand, no magnetic field is assumed present initially. On the walls, we assign

$$\mathbf{u}_j = \begin{pmatrix} 0 \\ 0 \end{pmatrix}, \text{ and } \mathbf{B}_j = \left(1 + \frac{(-1)^{j+1} \lceil j/2 \rceil}{5} \epsilon\right) \begin{pmatrix} 0 \\ 1 \end{pmatrix},$$

for the velocity, and magnetic field, respectively, where the applied magnetic field is normal to the flow direction. As the inflow conditions, at the inlet we set

$$\mathbf{u}_j = \left(1 + \frac{(-1)^{j+1} \lceil j/2 \rceil}{5} \epsilon\right) \begin{pmatrix} \frac{y(10-y)}{25} \\ 0 \end{pmatrix}, \text{ and } \mathbf{B}_j = \left(1 + \frac{(-1)^{j+1} \lceil j/2 \rceil}{5} \epsilon\right) \begin{pmatrix} 0 \\ 1 \end{pmatrix}.$$

For the outflow conditions, we extend the channel 10 units in the downstream direction and at the end we set outflow velocity and magnetic field equal to corresponding inflow conditions. Thus, ϵ appears as a perturbation parameter in the initial and boundary conditions. The initial and boundary conditions in the original variables are then transferred into the Elsässer variables. We generate a barycenter refined regular triangular unstructured mesh that provides a total of 186,134 velocity dofs, 23,395 pressure dofs, 186,134 magnetic field dofs, and 23,395 magnetic pressure dofs.

For this computational experiment, we consider a uniformly distributed random sample $\{(\nu_j, \nu_{m,j}) \in [0.0009, 0.0011] \times [0.009, 0.011]\}$ with mean $(\bar{\nu}, \bar{\nu}_m) = (0.001, 0.01)$, and no external source is considered in the system (i.e. $\mathbf{f}_j = \mathbf{g}_j = \mathbf{0}$). We run the simulations using the Algorithm 1 with a fixed coupling

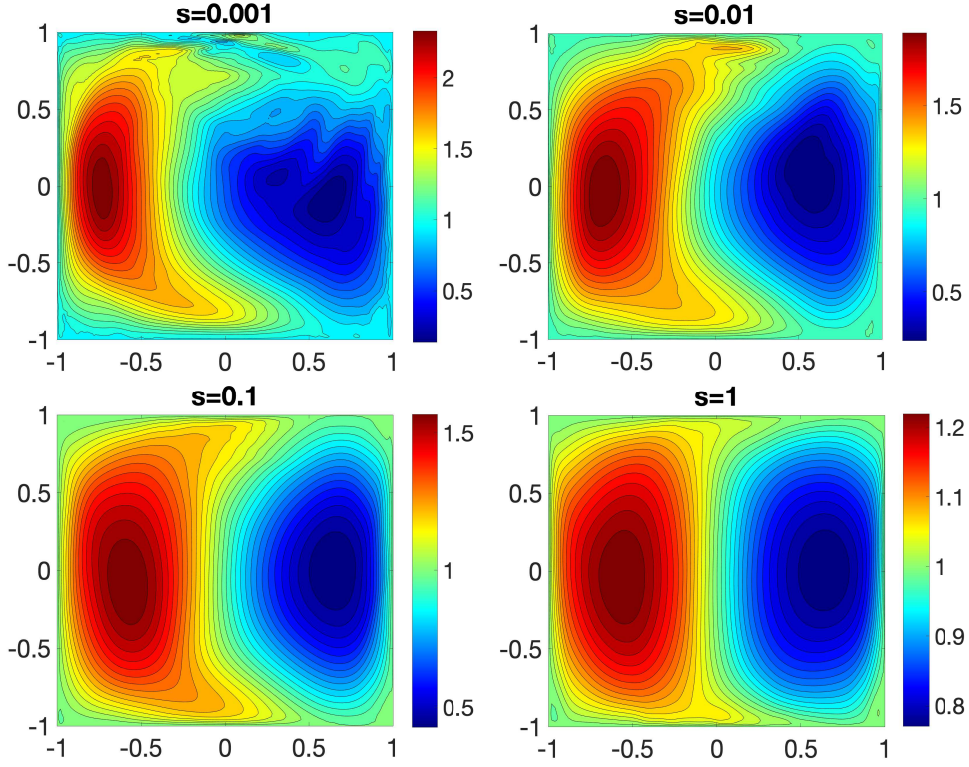


Fig. 4.4: A lid-driven cavity problem. The magnetic field strength ensemble average solutions for $13636.36 \leq Re_j \leq 16666.67$ at $T = 600$ for various coupling parameter s .

parameter $s = 0.001$, varying the perturbation parameter ϵ and a fixed time-step size $\Delta t = 0.05$ until an end time $T = 40$. We plot the velocity and magnetic field ensemble average solutions in Figures 4.5-4.6 for various values of ϵ . To make a comparison, we plot the solution for a single run simulation, which corresponds to the mean sample viscosities, and $\epsilon = 0.0$ and present as ‘usual MHD’ results. We observe that as $\epsilon \rightarrow 0$, the ensemble average solution converges to the usual MHD solution.

5. Conclusion and future works. In this paper, we have proposed, analyzed, and tested an efficient ensemble algorithm, for a set of MHD simulations, which has the following features: (1) The linearized stable scheme is decoupled into two smaller identical subproblems, which can be solved at each time-step, simultaneously. This decoupling allows solving potentially much bigger problems with complex geometries than the MHD algorithms in terms of the primitive variables. (2) At each time-step, the system matrix remains common to all the ensemble members with different right-hand-side vectors. As a result, huge saving in storage and computational time, because the memory allocation for the system matrix, its assembly, factorization/preconditioners are needed only once per time-step. Moreover, the advantage of a block linear solver can be taken. We assume the input data in the MHD flow involve uncertainties. Thus, each member of the set is corresponding to a distinct combination of kinematic viscosity, magnetic diffusivity, initial conditions, boundary conditions, and body force.

The unconditional stability of the scheme with respect to the time-step size is proven rigorously. The unconditional convergence is proven to be optimal in 2D, but in 3D the theory is suboptimal, due to the use of the inverse inequality in the analysis. It is unclear if the suboptimal convergence is true, or if the 3D analysis is not sharp. Numerical experiments are performed to verify the predicted convergence rates, and energy stability of the scheme. To observe the changes in the physical behavior as the coupling number increases we have implemented the scheme on a regularized lid-driven cavity with high Reynolds numbers. We observe how solution changes as the deviation of noise in the initial and boundary conditions increases on a channel flow past a rectangular step problems.

Our future work on MHD flow ensemble simulations will be based on Nédélec’s edge element [39] so

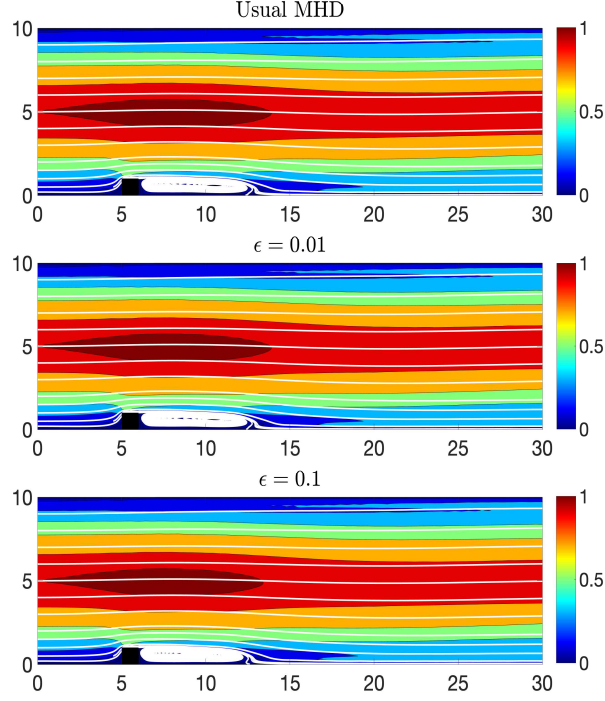


Fig. 4.5: The velocity ensemble average solutions (shown as streamlines over speed contour) at $T = 40$ for MHD channel flow over a step for $s = 0.001$.

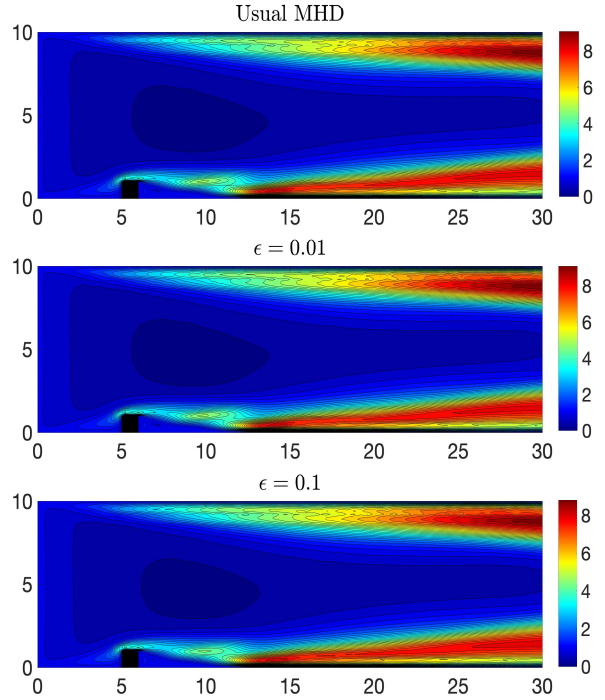


Fig. 4.6: The magnetic field strength ensemble average solutions at $T = 40$ for MHD channel flow over a step for $s = 0.001$.

that only the tangential component of the magnetic field becomes continuous across the inter-element boundaries. As a next step, this idea herein along with a penalty-projection [1] ensemble algorithm for each subproblem can be considered. For high order accurate uncertainty quantification along with

the ideas proposed in [34, 43] with deferred correction method will be the next research avenue. We will explore for more appropriate physical boundary conditions rather than the Dirichlet boundary conditions in Elsässer variables. It has been shown in [37], for Maxwell equations simulation, in presence of extremely different time scales, the iterative solver combination (FGMRES-GMRES) in conjunction with the parallel Auxiliary Space Maxwell (AMS) solver preconditioner outperforms over the direct solver. We plan to employ FGMRES-GMRES-AMS solver for solving complex problems using this scheme.

Parametric reduced order modeling (ROM) for MHD flow ensemble simulations following the data-driven approaches [25, 36, 44] and high order ROM differential filter in conjunction with evolve-filter-relax algorithm will also be the next research direction.

REFERENCES

- [1] M. Akbas, S. Kaya, M. Mohebujjaman, and L. Rebholz. Numerical analysis and testing of a fully discrete, decoupled penalty-projection algorithm for MHD in elsässer variable. *International Journal of Numerical Analysis & Modeling*, 13(1):90–113, 2016.
- [2] D. Arnold and J. Qin. Quadratic velocity/linear pressure Stokes elements. *Advances in Computer Methods for Partial Differential Equations*, 7:28–34, 1992.
- [3] M. J. Balajewicz, E. H. Dowell, and B. R. Noack. Low-dimensional modelling of high-Reynolds-number shear flows incorporating constraints from the Navier-Stokes equation. *Journal of Fluid Mechanics*, 729:285, 2013.
- [4] D. Biskamp. *Magnetohydrodynamic Turbulence*. Cambridge University Press, Cambridge, 2003.
- [5] S. C. Brenner and L. R. Scott. *The Mathematical Theory of Finite Element Methods*. Texts in Applied Mathematics, 15. Springer Science+Business Media, LLC, 2008.
- [6] P. A. Davidson. An introduction to magnetohydrodynamics. *Cambridge Texts in Applied Mathematics*, Cambridge University Press, Cambridge, 2001.
- [7] L. Fick, Y. Maday, A. T. Patera, and T. Taddei. A stabilized POD model for turbulent flows over a range of Reynolds numbers: Optimal parameter sampling and constrained projection. *Journal of Computational Physics*, 371:214–243, 2018.
- [8] J. A. Fiordilino and M. Winger. Unconditionally energy stable and first-order accurate numerical schemes for the heat equation with uncertain temperature-dependent conductivity. <https://arxiv.org/pdf/2106.02754.pdf>.
- [9] T. Fujita, D. J. Stensrud, and D. C. Dowell. Surface data assimilation using an ensemble Kalman filter approach with initial condition and model physics uncertainties. *Monthly Weather Review*, 135(5):1846–1868, 2007.
- [10] V. Girault and P.-A. Raviart. *Finite Element Methods for Navier-Stokes Equations: Theory and Algorithms*. Springer-Verlag, 1986.
- [11] M. Gunzburger, N. Jiang, and Z. Wang. An efficient algorithm for simulating ensembles of parameterized flow problems. *IMA Journal of Numerical Analysis*, 39(3):1180–1205, 2019.
- [12] M. Gunzburger, N. Jiang, and Z. Wang. A second-order time-stepping scheme for simulating ensembles of parameterized flow problems. *Computational Methods in Applied Mathematics*, 19(3):681–701, 2019.
- [13] F. Hecht. New development in Freefem++. *Journal of Numerical Mathematics*, 20:251–266, 2012.
- [14] T. Heister, M. Mohebujjaman, and L. Rebholz. Decoupled, unconditionally stable, higher order discretizations for MHD flow simulation. *Journal of Scientific Computing*, 71:21–43, 2017.
- [15] J. G. Heywood and R. Rannacher. Finite-Element approximation of the nonstationary Navier-Stokes problem part IV: error analysis for second-order time discretization. *SIAM Journal on Numerical Analysis*, 27:353–384, 1990.
- [16] K. Hu, Y. Ma, and J. Xu. Stable finite element methods preserving $\nabla \cdot B = 0$ exactly for MHD models. *Numerische Mathematik*, 135:371–397, 2017.
- [17] N. Jiang. A higher order ensemble simulation algorithm for fluid flows. *Journal of Scientific Computing*, 64:264–288, 2015.
- [18] N. Jiang. A second-order ensemble method based on a blended backward differentiation formula timestepping scheme for time-dependent Navier–Stokes equations. *Numerical Methods for Partial Differential Equations*, 33(1):34–61, 2017.
- [19] N. Jiang, S. Kaya, and W. Layton. Analysis of model variance for ensemble based turbulence modeling. *Computational Methods in Applied Mathematics*, 15:173–188, 2015.
- [20] N. Jiang and W. Layton. An algorithm for fast calculation of flow ensembles. *International Journal for Uncertainty Quantification*, 4:273–301, 2014.
- [21] N. Jiang and W. Layton. Numerical analysis of two ensemble eddy viscosity numerical regularizations of fluid motion. *Numerical Methods for Partial Differential Equations*, 31:630–651, 2015.
- [22] N. Jiang, Y. Li, and H. Yang. An artificial compressibility Crank–Nicolson leap-frog method for the Stokes–Darcy model and application in ensemble simulations. *SIAM Journal on Numerical Analysis*, 59(1):401–428, 2021.
- [23] N. Jiang and M. Schneier. An efficient, partitioned ensemble algorithm for simulating ensembles of evolutionary MHD flows at low magnetic Reynolds number. *Numerical Methods for Partial Differential Equations*, 34(6):2129–2152, 2018.
- [24] L. Ju, W. Leng, Z. Wang, and S. Yuan. Numerical investigation of ensemble methods with block iterative solvers for evolution problems. *Discrete & Continuous Dynamical Systems-B*, 25(12):4905, 2020.
- [25] A. A. Kaptanoglu, K. D. Morgan, C. J. Hansen, and S. L. Brunton. Physics-constrained, low-dimensional models for magnetohydrodynamics: First-principles and data-driven approaches. *Physical Review E*, accepted, 2021.
- [26] L. D. Landau and E. M. Lifshitz. *Electrodynamics of Continuous Media*. Pergamon Press, Oxford, 1960.
- [27] W. Layton, C. C. Manica, M. Neda, and L. G. Rebholz. Numerical analysis and computational testing of a high

- accuracy Leray-deconvolution model of turbulence. Numerical Methods for Partial Differential Equations: An International Journal, 24(2):555–582, 2008.
- [28] M. W. Lee, E. H. Dowell, and M. J. Balajewicz. A study of the regularized lid-driven cavity’s progression to chaos. Communications in Nonlinear Science and Numerical Simulation, 71:50–72, 2019.
 - [29] J. M. Lewis. Roots of ensemble forecasting. Monthly Weather Review, 133:1865 – 1885, 2005.
 - [30] N. Jiang M. Gunzburger and Z. Wang. A second-order time-stepping scheme for simulating ensembles of parameterized flow problems. Computational Methods in Applied Mathematics, 1(4):349–364, 1988.
 - [31] T. N. Palmer M. Leutbecher. Ensemble forecasting. Journal of Computational Physics, 227:3515–3539, 2008.
 - [32] O. P. L. Maître and O. M. Knio. Spectral methods for uncertainty quantification. Springer, 2010.
 - [33] W. J. Martin and M. Xue. Sensitivity analysis of convection of the 24 May 2002 IHOP case using very large ensembles. Monthly Weather Review, 134(1):192–207, 2006.
 - [34] M. Mohebujjaman. High order efficient algorithm for computation of MHD flow ensembles. Advances in Applied Mathematics and Mechanics, accepted, 2021.
 - [35] M. Mohebujjaman and L. G. Rebholz. An efficient algorithm for computation of MHD flow ensembles. Computational Methods in Applied Mathematics, 17:121–137, 2017.
 - [36] M. Mohebujjaman, L. G. Rebholz, and T. Iliescu. Physically-constrained data-driven, filtered reduced order modeling of fluid flows. International Journal for Numerical Methods in Fluids, 89(3):103–122, 2019.
 - [37] M. Mohebujjaman, S. Shiraiwa, B. LaBombard, J. C. Wright, and K. Uppalapati. Scalability analysis of direct and iterative solvers used to model charging of non-insulated superconducting pancake solenoids. arXiv preprint arXiv:2007.15410, 2020.
 - [38] M. Neda, A. Takhirov, and J. Waters. Ensemble calculations for time relaxation fluid flow models. Numerical Methods for Partial Differential Equations, 32(3):757–777, 2016.
 - [39] J. C. Nédélec. Mixed finite elements in \mathbb{R}^3 . Numerische Mathematik, 35(3):315–341, 1980.
 - [40] J. D. Giraldo Osorio and S. G. Garcia Galiano. Building hazard maps of extreme daily rainy events from PDF ensemble, via REA method, on Senegal river basin. Hydrology and Earth System Sciences, 15:3605 – 3615, 2011.
 - [41] J. C. Robinson, J. L. Rodrigo, and W. Sadowski. The Three-Dimensional Navier-Stokes Equations. Cambridge University Press, 2016.
 - [42] C. Trenchea. Unconditional stability of a partitioned IMEX method for magnetohydrodynamic flows. Applied Mathematics Letters, 27:97–100, 2014.
 - [43] N. Wilson, A. Labovsky, and C. Trenchea. High accuracy method for magnetohydrodynamics system in Elsässer variables. Computational Methods in Applied Mathematics, 15(1):97–110, 2015.
 - [44] X. Xie, M. Mohebujjaman, L. G. Rebholz, and T. Iliescu. Data-driven filtered reduced order modeling of fluid flows. SIAM Journal on Scientific Computing, 40(3):B834–B857, 2018.
 - [45] S. Zhang. A new family of stable mixed finite elements for the 3D Stokes equations. Mathematics of Computation, 74:543–554, 2005.
 - [46] Y. Zhang. Critical transition Reynolds number for plane channel flow. Applied Mathematics and Mechanics, 38(10):1415–1424, 2017.